J. Fluid Mech. (2000), *vol.* 405, *pp.* 211–241. Printed in the United Kingdom

Instability of two annular layers or a liquid thread bounded by an elastic membrane

By C. POZRIKIDIS

University of California, San Diego, La Jolla, Ca 92093-0411, USA
e-mail: cpozrikidis@.ucsd.edu

(Received 26 January 1999 and in revised form 12 October 1999)

The instability of an annular layer coated on the interior side of an outer circular tube and surrounding another annular layer coated on the exterior side of an inner circular tube, is studied in the absence of an imposed flow due to a pressure gradient or boundary motion. As the radius of the inner cylinder tends to vanish and the radius of the outer cylinder tends to infinity, the inner layer reduces to a liquid thread suspended in a quiescent infinite ambient fluid. The fluids are separated by a membrane that exhibits constant surface tension and develops elastic tensions due to deformation from the unstressed cylindrical shape. The surface tension is responsible for the Rayleigh capillary instability, but the elastic tensions resist the deformation and slow down or even prevent the growth of small perturbations. In the first part of this paper, we formulate the linear stability problem for axisymmetric perturbations, and derive a nonlinear eigenvalue system whose solution produces the complex phase velocity of the normal modes. When inertial effects are negligible, there are two normal modes; one is stable under any conditions, and the second may be unstable when the interfacial elasticity is sufficiently small compared to surface tension, and the wavelength of the perturbation is sufficiently long. Stability graphs are presented to illustrate the properties of the normal modes and their dependence on the ratio of the viscosity of the outer to inner fluid, the interfacial elasticity, and the ratios of the cylinders' radii to the interface radius. The results show that as the interfacial elasticity tends to vanish, the unconditionally stable mode becomes physically irrelevant by requiring extremely large ratios of axial to lateral displacement of material points along the trace of the membrane in an azimuthal plane. In the second part of this paper, we investigate the nonlinear instability of an infinite thread in the limit of vanishing Reynolds numbers by dynamical simulation based on a boundary-integral method. In the problem formulation, the elastic tensions derive from a constitutive equation for a thin sheet of an incompressible isotropic elastic solid described by Mooney's constitutive law. The numerical results suggest that the interfacial elasticity ultimately restrains the growth of disturbances and leads to slowly evolving periodic shapes, in agreement with laboratory observations.

1. Introduction

The instability of cylindrical interfaces due to surface tension has received considerable attention since Plateau's (1873) observations of the breakup of liquid jets, and the classical analyses of Rayleigh (1878, 1892), as reviewed by Yarin (1993), Papageorgiou (1996), Eggers (1997), Lin & Reitz (1998). Much less attention has been devoted to cylindrical interfaces that do not simply mark the boundary between

two fluids, but have a distinct structure that is responsible for non-isotropic tensions. Such interfaces are known to arise in several biological and biophysical contexts, as discussed by Lipowsky (1991), Nelson, Powers & Seifert (1995), and Seifert (1997). For example, axisymmetric unduloidal shapes with constant mean curvature, including those assumed by certain foraminifera, and the myelin figures found inside and outside aged red blood cells, have been speculated to result from the instability of cylindrical membrane tubules.

In this work, we consider the instability of cylindrical interfaces with a membrane-like constitution that is responsible for non-isotropic and deformation-dependent tension. In practice, these membranes may be identified with grossly polluted or polymerized interfaces of elongated capsules. In biophysical and physiological applications, these membranes may be identified with single or lamellar composites of lipid bilayers, possibly in the presence of a supporting protein network. Examples are the network comprising the cytoskeleton of red blood cells and the capsular shell of eukaryotic organisms.

The mechanical behaviour of a membrane depends strongly on its constitution. If the fluids on either side of a membrane are immiscible, surface tension is established as the result of chemical asymmetry, that is, differences in attractive molecular forces between the two species. Surfactant molecules diminish these differences and render the surface tension a function of the local surfactant concentration. Polymerized membranes develop stress resultants, that is elastic tensions, and bending moments similar to those exhibited by thin elastic shells. The bilayer of the membrane of red blood cells is responsible for incompressible behaviour, whereas the cytoskeleton is responsible for elastic behaviour that causes the cell to return to the resting shape of a biconcave disk (e.g. Mohandas & Evans 1994). When subjected to hydrodynamic traction, the membrane develops a position-dependent isotropic tension which ensures that the deformation preserves the surface area of material patches over the membrane.

Zarda, Chien & Skalak (1977) computed large elastic deformations of red blood cells on the basis of a model that includes the elasticity of the membrane under tension in its own plane, as well bending moments. Several authors have used lubrication flow models to describe the motion of tightly fitting deformable particles through capillary tubes, as reviewed by Secomb & Hsu (1993). Small and large deformations of solitary and suspensions of capsules enclosed by elastic membranes, modelling red blood cells, were studied by Barthès-Biesel (1980), Barthès-Biesel & Rallison (1981), Li, Barthès-Biesel & Helmy (1988), Pozrikidis (1995), Ramanujan & Pozrikidis (1998), Navot (1998), Eggleton & Popel (1998), and Breyiannis & Pozrikidis (1999). The statics and dynamics of fluid-containing elastic shells have been studied extensively in the laboratory and by numerical simulation with reference to the oscillations and collapse of elastic vessels in biomechanics (e.g. Pedley & Luo 1998; Heil 1997, 1999*a*,*b*).

Membranes consisting of lipid bilayers exhibit bending elasticity, that is resistance to bending from an equilibrium configuration. The equilibrium shape of membranes consisting of a symmetric bilayer possesses zero mean curvature. The surface tension of these membranes incorporates two contributions: one associated with a surface energy that is proportional to the membrane surface area, and an entropic tension associated with the membrane's wrinkled shape due to thermal fluctuations. The application of an external tension to counteract the entropic tension smooths out the corrugated shapes and reveals an unfolded area that increases with tension at a logarithmic rate. To a first approximation, the energy stored in a membrane consisting of a symmetric bilayer can be set equal to the sum of the total surface area multiplied

by the surface tension, and the integral of the square of the mean curvature multiplied by twice the membrane bending stiffness (Lipowsky 1991).

Pozrikidis (1990), Zhou & Pozrikidis (1995), Kraus *et al.* (1996), and Seifert (1998) computed the deformation of vesicles enclosed by incompressible membranes subject to a straining or simple shear flow. Kraus *et al.* (1996) and Seifert (1998) accounted for the bending moments by setting the jump in the interfacial hydrodynamic traction equal to the gradient of an appropriate membrane energy function. More recently, Boey, Boal & Discher (1998*a*,*b*) developed a coarse-grained molecular model that permits the direct coupling of classical hydrodynamics to the dynamics of the molecular layers and networks comprising the membrane, in a manner that circumvents the explicit use of a macroscopic constitutive equation.

Relevant to the subject of the present work is the laboratory study of Bar-Ziv & Moses (1994) who excited stable cylindrical bilayer membranes of radii 0.3 to 5 μm and length a few hundred μm by the use of laser tweezers, and observed an instability that causes the formation of sinusoidal corrugations with suppressed thermal fluctuations. In physical terms, the laser spot causes local heating that produces strong electric field gradients which pull the bilayer toward the spot, thereby generating significant surface tension that initiates a capillary instability. When the wave amplitude has grown to a sufficiently large level, bending moments arrest its growth. Bar-Ziv & Moses (1994) observed that the reduced wavenumber ka of the 'pearling' state lies in the range $(0.64, 1)$, with typical value of 0.8, and used this observation to compute the entropic tension based on membrane energy consideration; k is the wavenumber and a is the thread radius. Bar-Ziv & Moses (1994) observed that the stronger application of the tweezers gives rise to a pearling conformation consisting of isolated, nearly spherical vesicles travelling along thin tubes towards the point where the tweezers have been applied. When the tweezers are released, the periodic corrugation immediately disappears to yield the cylindrical shape. The pearling configuration disppears gradually as surface-tension relaxation waves travel through the narrow stems. These experiments clearly demonstrate that a certain amount of sustained surface tension is able to induce long-lived or even permanent deformation. Nelson *et al.* (1995) proposed a model for predicting the wavelength of the corrugations seen in the experiments, accounting for the hydrodynamics of the bilayer under tension.

The experiments of Bar-Ziv & Moses (1994) involve a hydrodynamic system that is governed by a destabilizing mechanism associated with surface tension, and a stabilizing mechanism due to elastic membrane behaviour. Our goal in this paper is to study the interplay between these two mechanisms on the basis of a prototypical configuration. We consider, in particular, the instability of a cylindrical interface between two viscous fluids in the presence of a uniform and time-independent surface tension, and subject to elastic tensions developing due to the deformation. For the sake of generality, we also account for the presence of an inner coaxial cylinder that may be regarded as a model of a cell nucleus, and an outer coaxial cylinder that may be regarded as the surface of a boundary.

Halpern & Grotberg (1992, 1993) studied the dynamics of a thin film coated on the inner surface of an elastic tube modelling a bronchiole, taking into consideration the presence of surfactants. Using an asymptotic model that incorporates the lubrication approximation for the fluid flow and a small-deflection approximation for the wall tensions, they showed that one of the following possibilities may occur: a liquid bridge may form occluding the bronchiole; the wall may collapse when the surface tension is sufficient high or the wall modulus of elasticity is sufficiently low; or both occlusion

and collapse may occur. The physical system studied by Halpern & Grotberg (1992, 1993) is similar to that considered in the present study, in the sense that both involve the destabilizing action of surface tension and stabilizing elastic tensions. Differences, however, exist in both methods of analysis and physical application. Most important, the absence of interfacial elasticity in the system of Halpern & Grotberg does not allow the perturbations to evolve toward a steady or slowly evolving shape.

Several authors have studied the collapse of an elastic tube occurring when the external pressure is higher than the internal pressure, that is under negative transmural pressure (e.g. Pedley & Luo 1998; Heil 1997, 1998). In the mathematical modelling, the tube is assumed to develop in-plane elastic tensions as well as bending moments due to the deformation from a specified unstressed configuration. When the magnitude of a negative transmural pressure is sufficiently large, non-axisymmetric buckling occurs and the tube assumes a pinched shape. There are obvious similarities between the collapse of an elastic tube and the instability of an elastic interface. One important difference is that in the case of an elastic tube, the transmural pressure is positive, its magnitude being determined by the tube radius and the surface tension. Thus, when the surface tension vanishes instability does not arise.

In the first part of this paper, we carry out a linear stability analysis of a cylindrical interface between two viscous fluids subject to axisymmetric perturbations, and demonstrate explicitly the stabilizing effect of the elastic tensions. In the limit of vanishing Reynolds number and in the presence of interfacial elasticity, we obtain two normal modes with different ratios of the axial to lateral displacement of material points over the trace of the membrane in an azimuthal plane. In the second part of this paper, we study the nonlinear stages of the instability of a thread in the limit of vanishing Reynolds number by means of numerical simulations using the boundary-integral method for Stokes flow. For simplicity, we assume that the interface elasticity is adequately described by a constitutive equation corresponding to a thin sheet of an isotropic elastic and incompressible material obeying Mooney's constitute law. The results of the simulations demonstrate explicitly how the competition between a stabilizing and a destabilizing mechanism may lead to perfect or slowly evolving equilibrium shapes similar to those observed in the aforementioned experiments.

2. Linear stability analysis for Navier–Stokes flow

We consider the instability of an annular viscous layer coated on the interior surface of an outer circular cylinder, and surrounding a core fluid coated on the exterior surface of an inner circular cylinder, as illustrated in figure 1. As the radius of the inner cylinder tends to vanish and the radius of the outer cylinder tends to infinity, the core reduces to an infinite thread suspended in an infinite quiescent ambient fluid. We assume that the two fluids are separated by a membrane with infinitesimal thickness that exhibits time-independent and uniform surface tension, and develops elastic tensions due to deformation from the unstressed shape. In the unperturbed cylindrical state, the fluids are stationary and the elastic tensions vanish.

We begin by introducing cylindrical polar coordinates (x, σ, φ), with the x-axis coinciding with the axis of the thread or annular layer, as shown in figure 1. In the unperturbed state, the interface has a perfectly cylindrical shape with a circular cross-section of radius a. To carry out a normal-mode analysis, we describe the radial position of the interface as

$$\sigma = f(x,t) = a + \varepsilon a_1 \exp(\mathrm{i}k(x - ct)), \tag{2.1}$$

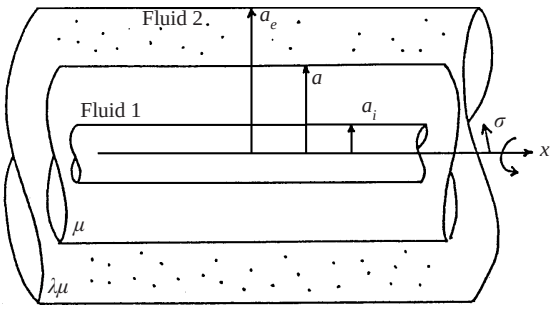

FIGURE 1. Illustration of an annular layer coated on the interior surface of an outer circular tube and surrounding another annular layer coated on the exterior surface of an inner circular tube. The two fluids are separated by a membrane that exhibits constant surface tension and develops elastic tensions due to deformation from the cylindrical shape.

where ε is a dimensionless coefficient whose magnitude is much less than unity, a_1 is the complex amplitude of the interfacial perturbation, i is the imaginary unit, $k = 2\pi/L$ is the wavenumber, L is the wavelength, and c is the complex phase velocity.

The motion of the fluid on either side of the interface is governed by the continuity equation and the Navier–Stokes equation with appropriate constants corresponding to the physical properties of the two fluids. Taking advantage of the assumed axial symmetry of the flow, we describe the perturbation flow in terms of the Stokes stream function Ψ_j, where $j = 1$ or 2 for the inner or outer fluid respectively. The axial and radial components of the velocity are given by

$$u_{xj} = \varepsilon \frac{1}{\sigma} \frac{\partial \Psi_j}{\partial \sigma}, \quad u_{\sigma j} = -\varepsilon \frac{1}{\sigma} \frac{\partial \Psi_j}{\partial x}. \tag{2.2}$$

The azimuthal component of the vorticity is given by

$$\omega_{\varphi j} = -\varepsilon \frac{1}{\sigma} \mathrm{D}^2 \Psi_j, \tag{2.3}$$

where D^2 is a second-order differential operator defined as

$$\mathrm{D}^2 = \frac{\partial^2}{\partial x^2} + \frac{\partial^2}{\partial \sigma^2} - \frac{1}{\sigma} \frac{\partial}{\partial \sigma}. \tag{2.4}$$

Substituting these expressions into the azimuthal component of the vorticity transport equation, and linearizing the resulting expression with respect to ε, we derive the fourth-order partial differential equation

$$\mathrm{E}_j^2 \mathrm{D}^2 \Psi_j = 0, \tag{2.5}$$

where E_j^2 is another second-order differential operator defined as

$$\mathrm{E}_j^2 = \mathrm{D}^2 - \frac{1}{v_j} \frac{\partial}{\partial t} \tag{2.6}$$

and v_j is the kinematic viscosity of the jth fluid.

We proceed by expressing the perturbation stream function in the usual normal-mode form

$$\Psi_j = \phi_j(\sigma) \exp(\mathrm{i}k(x - ct)). \tag{2.7}$$

Substituting this expression into (2.5), we derive a fourth-order ordinary differential equation for the functions ϕ_j. The general solution was given by Tomotika (1935) in the form

$$\phi_j(\sigma) = \sigma(A_{1,j} I_1(k\sigma) + B_{1,j} K_1(k\sigma) + A_{2,j} I_1(k_j\sigma) + B_{2,j} K_1(k_j\sigma)), \tag{2.8}$$

where $A_{1,j}$ and $B_{1,j}$ are constant coefficients, I_1, K_1 are modified Bessel functions of the first kind, and we have introduced the modified wavenumbers defined by

$$k_j^2 \equiv k^2 - \frac{\mathrm{i}ck}{\nu_j}. \tag{2.9}$$

The pressure may be expressed in the corresponding form

$$p_j = \varepsilon \Pi_j(\sigma) \exp(\mathrm{i}k(x - ct)). \tag{2.10}$$

Substituting equations (2.2), (2.7), (2,8), and (2.9) into the x-component of the Navier–Stokes equation, and linearizing with respect to ε, we find

$$\Pi_j(\sigma) = -ck\rho_j(A_{1,j} I_0(k\sigma) - B_{1,j} K_0(k\sigma)). \tag{2.11}$$

Next, we consider the implementation of the kinematic and dynamic boundary conditions at the interface. Continuity of velocity requires $\phi_1 = \phi_2$ and $\mathrm{d}\phi_1/\mathrm{d}\sigma = \mathrm{d}\phi_2/\mathrm{d}\sigma$ at $\sigma = f(x, t)$, where the function $f(x, t)$, determining the location of the interface, was introduced in equation (2.1). Applying domain perturbation linearization, we derive the linearized conditions

$$\phi_1(a) = \phi_2(a), \quad \left(\frac{\mathrm{d}\phi_1}{\mathrm{d}\sigma}\right)_{\sigma=a} = \left(\frac{\mathrm{d}\phi_2}{\mathrm{d}\sigma}\right)_{\sigma=a}. \tag{2.12}$$

The evolution of the deforming interface must be consistent with the motion of the fluid on either side of the interface. The requirement that fluid point particles lying in the interface do not penetrate the bulk of the fluids imposes the condition

$$\frac{\partial f}{\partial t} + u_x \frac{\partial f}{\partial x} - u_\sigma = 0, \tag{2.13}$$

where all functions are evaluated at the location of the unperturbed interface. Substituting equations (2.1), (2.2), and (2.7) into equation (2.13), applying once again the method of domain perturbation, and discarding terms that do not depend linearly on ε, we find the following expression for the complex amplitude of the perturbation:

$$a_1 = \frac{1}{ac} \phi_j(\sigma = a), \tag{2.14}$$

where, in view of (2.12), we may set $j = 1$ or 2 on the right-hand side.

To satisfy the kinematic boundary conditions on the surface of the cylinders, we require

$$u_{x,1} = \left(\frac{1}{\sigma}\frac{\partial \Psi_1}{\partial \sigma}\right)_{\sigma=a_i} = 0, \quad u_{\sigma,1} = -\left(\frac{1}{\sigma}\frac{\partial \Psi_1}{\partial x}\right)_{\sigma=a_i} = 0 \tag{2.15}$$

and

$$u_{x,2} = \left(\frac{1}{\sigma}\frac{\partial \Psi_2}{\partial \sigma}\right)_{\sigma=a_e} = 0, \quad u_{\sigma,2} = -\left(\frac{1}{\sigma}\frac{\partial \Psi_2}{\partial x}\right)_{\sigma=a_e} = 0, \tag{2.16}$$

where a_i, a_e are the radii of the inner and outer cylinders, respectively, as shown in figure 1.

The dynamic interfacial condition requires that the jump in the hydrodynamic traction be balanced by the normal stress due to the surface tension γ, as well as by the normal and tangential stress due to the elastic tensions, so that

$$\Delta \boldsymbol{f} \equiv (\boldsymbol{\sigma}^{(1)} - \boldsymbol{\sigma}^{(2)}) \cdot \boldsymbol{n} = 2\kappa_m \gamma \boldsymbol{n} + \Delta \boldsymbol{f}^{Els}, \tag{2.17}$$

where $\boldsymbol{\sigma}^{(1)}$, $\boldsymbol{\sigma}^{(2)}$ are the hydrodynamic stress tensors for the inner or outer fluid, $\boldsymbol{n}$ is the unit vector normal to the interface pointing into the inner fluid labelled 1, and κ_m is the mean curvature of the interface. A force balance over a small section of the interface shows that the jump in the hydrodynamic traction due to the elastic tensions is given by

$$\Delta \boldsymbol{f}^{Els} = (\kappa_l \tau_{ll} + \kappa_\varphi \tau_{\varphi\varphi})\boldsymbol{n} - \left(\frac{\partial \tau_{ll}}{\partial l} + \frac{1}{\sigma} \frac{\partial \sigma}{\partial l} (\tau_{ll} - \tau_{\varphi\varphi}) \right) \boldsymbol{t}, \tag{2.18}$$

where κ_l, κ_φ are the principal curvatures of the interface in the azimuthal plane and its conjugate plane, τ_{ll}, $\tau_{\varphi\varphi}$ are the principal elastic tensions referring to orthogonal curvilinear axes corresponding to the tangential vector $\boldsymbol{t}$ and the azimuthal angle φ, and l is the arclength measured in the direction of $\boldsymbol{t}$ (e.g. Pozrikidis 1992, pp. 152–153). Surface moment resultants are required to satisfy the torque balance in the presence of transverse shearing tension, but these are assumed to be negligible due to the small thickness of the membrane (e.g. Zarda *et al.* 1977; Evans & Yeung 1994).

All functions in equations (2.17) and (2.18) are evaluated at the position of the unperturbed interface. Using equation (2.1) and standard expressions for the normal vector and curvatures (e.g. Pozrikidis 1997), we derive the linearized forms

$$\boldsymbol{n} = -\boldsymbol{e}_\sigma + \varepsilon \mathrm{i} k a_1 \exp(\mathrm{i}k(x - ct))\boldsymbol{e}_x, \tag{2.19}$$

where $\boldsymbol{e}_x$ and $\boldsymbol{e}_\sigma$ are the unit vectors in the axial and radial directions, and

$$\left.\begin{aligned} &\kappa_l = -\varepsilon a_1 k^2 \exp(\mathrm{i}k(x - ct)), \quad \kappa_\varphi = -\frac{1}{a} + \varepsilon \frac{a_1}{a^2} \exp(\mathrm{i}k(x - ct)), \\ &2\kappa_m = \kappa_l + \kappa_\varphi = -\frac{1}{a} + \varepsilon \frac{a_1}{a^2}(1 - k^2 a^2) \exp(\mathrm{i}k(x - ct)). \end{aligned}\right\} \tag{2.20}$$

Next, we express the linearized principal elastic tensions in the normal-mode forms

$$\tau_{ll} = \varepsilon \gamma_l \exp(\mathrm{i}k(x - ct)), \quad \tau_{\varphi\varphi} = \varepsilon \gamma_\varphi \exp(\mathrm{i}k(x - ct)), \tag{2.21}$$

where γ_l and γ_φ are complex coefficients to be determined as part of the solution. Substituting these forms along with expressions (2.19)–(2.21) into (2.18), the result into (2.17), and linearizing both sides with respect to ε, we obtain the following two scalar linearized boundary conditions for the tangential and normal components of the traction:

$$\mu_1 \left(\frac{\partial u_{x,1}}{\partial \sigma} + \frac{\partial u_{\sigma,1}}{\partial x} \right) - \mu_2 \left(\frac{\partial u_{x,2}}{\partial \sigma} + \frac{\partial u_{\sigma,2}}{\partial x} \right) = \varepsilon \mathrm{i} k \gamma_l \exp(\mathrm{i}k(x - ct)) \tag{2.22}$$

and

$$-p_1 + 2\mu_1 \frac{\partial u_{\sigma,1}}{\partial \sigma} + p_2 - 2\mu_2 \frac{\partial u_{\sigma,2}}{\partial \sigma} = \varepsilon \left(-\gamma_0 \frac{a_1}{a^2}(1 - k^2 a^2) + \gamma_\varphi \frac{1}{a} \right) \exp(\mathrm{i}k(x - ct)), \tag{2.23}$$

where both sides are evaluated at the location of the unperturbed interface, at $\sigma = a$.

To this end, we require a constitutive equation relating the elastic tensions to the interfacial deformation. For this purpose, we introduce the principal extension ratios

$$\lambda_l = \frac{\partial l}{\partial l_U}, \quad \lambda_\varphi = \frac{\sigma}{\sigma_U}, \tag{2.24}$$

where the subscript U signifies the unstressed state. Assuming that the membrane behaves like a thin elastic sheet of an incompressible material that obeys the Mooney constitutive law, we write

$$\tau_{ll} = \tfrac{2}{3}E(2\hat{\lambda}_l + \hat{\lambda}_\varphi), \quad \tau_{\varphi\varphi} = \tfrac{2}{3}E(\hat{\lambda}_l + 2\hat{\lambda}_\varphi), \tag{2.25a,b}$$

where E is the modulus of elasticity, $\hat{\lambda}_l \equiv \lambda_l - 1$, and $\hat{\lambda}_\varphi \equiv \lambda_\varphi - 1$ (Green & Adkins 1960; Li *et al.* 1988; McDonald 1996). Introducing the normal-mode expansions

$$\lambda_l = 1 + \varepsilon\chi_l \exp(\mathrm{i}k(x - ct)), \quad \lambda_\varphi = 1 + \varepsilon\chi_\varphi \exp(\mathrm{i}k(x - ct)) \tag{2.26a,b}$$

and substituting them along with expressions (2.21) into equations (2.25), we find

$$\gamma_l = \tfrac{2}{3}E(2\chi_l + \chi_\varphi), \quad \gamma_\varphi = \tfrac{2}{3}E(\chi_l + 2\chi_\varphi). \tag{2.27}$$

It remains to derive evolution equations for the principal extension ratios. An evolution equation for λ_φ arises simply by substituting (2.1) into (2.25b) and setting σ_U equal to the unperturbed radius of the interface a to obtain

$$\chi_\varphi = \frac{a_1}{a}. \tag{2.28}$$

The evolution equation for χ_l derives from the equation of motion of a material vector lying along the trace of the interface in an aximuthal plane,

$$\frac{1}{\chi_l}\frac{\mathrm{D}\chi_l}{\mathrm{D}t} = \boldsymbol{t}\cdot\boldsymbol{L}\cdot\boldsymbol{t} \tag{2.29}$$

where $\mathrm{D}/\mathrm{D}t$ is the material derivative, and $\boldsymbol{L}$ is the velocity gradient tensor (e.g. Pozrikidis 1997, Chap. 1). Linearizing equation (2.29) we find

$$\chi_l = -\frac{1}{ca}\left(\frac{\partial\phi_j}{\partial\sigma}\right)_{\sigma=a}, \tag{2.30}$$

where $j = 1$ or 2.

We recall that the interface has been assumed to be unstressed when it has a cylindrical shape, set the right-hand side of (2.25a) equal to the right-hand side of (2.26a), and substitute equation (2.30) into the result. Integrating the emerging expression with respect to x, we find that the axial displacement of a material membrane point which at the unstressed state was located at x, is given by

$$\delta X = \varepsilon\frac{\mathrm{i}}{kca}\left(\frac{\partial\phi_j}{\partial\sigma}\right)_{\sigma=a} \exp(\mathrm{i}k(x - ct)), \tag{2.31}$$

where $j = 1$ or 2. The corresponding radial displacement, as given by equation (2.28), is given by

$$\delta\Sigma = \varepsilon a_1 \exp(\mathrm{i}k(x - ct)). \tag{2.32}$$

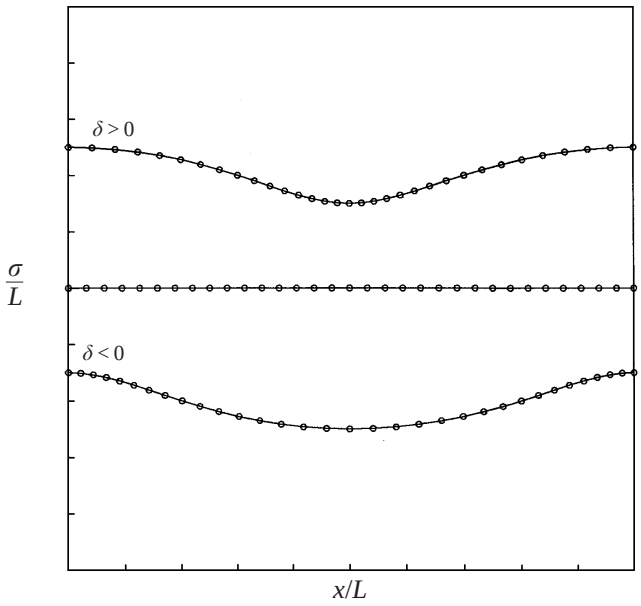

FIGURE 2. Position of point particles along the membrane for a normal-mode perturbation leading to exponential decay or growth, for positive and negative values of the displacement ratio δ. In the unperturbed state, the particles are distributed evenly along the x-axis, as shown in the middle of the illustration.

We anticipate now that, because of the absence of a mean flow, the phase velocity c will be purely imaginary, and select the real parts of the preceding two equations to obtain the normal mode parametrization

$$X = x + \varepsilon X_1 \sin(kx) \exp(-\mathrm{i}kct), \quad \Sigma = a + \varepsilon \Sigma_1 \cos(kx) \exp(-\mathrm{i}kct), \tag{2.33}$$

where we have defined

$$X_1 \equiv \frac{1}{\mathrm{i}kca} \left(\frac{\partial \phi_j}{\partial \sigma} \right)_{\sigma = a}, \quad \Sigma_1 \equiv a_1. \tag{2.34}$$

The ratio of the axial and radial amplitudes

$$\delta \equiv \frac{X_1}{\Sigma_1} = -\frac{1}{(-\mathrm{i}kc)aa_1} \left(\frac{\partial \phi_j}{\partial \sigma} \right)_{\sigma = a} \tag{2.35}$$

determines the direction of displacement of the individual material points corresponding to the normal modes. Figure 2 illustrates the perturbed position of point particles which in the unstressed state are distributed evenly along the trace of the membrane, as shown in the middle of the figure, for a positive and a negative value of δ.

Collecting the kinematic and dynamic boundary conditions expressed by equations (2.14), (2.15), (2.16), (2.22), and (2.23), and using the derived expressions for the velocity, pressure, curvatures, and elastic tensions, we formulate the following system of eight homogeneous equations for the eight unknown coefficients $A_{i,j}$ and $B_{i,j}$ for $i, j = 1, 2$:

$$\boldsymbol{M}\boldsymbol{w} = \boldsymbol{0}, \tag{2.36}$$

where $\mathbf{0}$ is a null vector, $\boldsymbol{w}$ is a vector of unknown coefficients defined as

$$\boldsymbol{w} = [A_{1,1}, A_{2,1}, B_{1,1}, B_{2,1}, A_{1,2}, A_{2,2}, B_{1,2}, B_{2,2}] \tag{2.37}$$

and

$$\boldsymbol{M} = \begin{bmatrix} I_1(ka) & I_1(k_1a) & K_1(ka) & K_1(k_1a) \\ kI_0(ka) & k_1I_0(k_1a) & -kK_0(la) & -k_1K_0(k_1a) \\ I_1(ka_i) & I_1(k_1a_i) & K_1(ka_i) & K_1(k_1a_i) \\ kI_0(ka_i) & k_1I_0(k_1a_i) & -kK_0(ka_i) & -k_1K_0(k_1a_i) \\ 0 & 0 & 0 & 0 \\ 0 & 0 & 0 & 0 \\ F_1 & F_2 & F_3 & F_4 \\ G_1 & G_2 & G_3 & G_4 \end{bmatrix}$$

$$\begin{bmatrix} -I_1(ka) & -I_1(k_2a) & -K_1(ka) & -K_1(k_2a) \\ -kI_0(ka) & -k_2I_0(k_2a) & kK_0(ka) & k_2K_0(k_2a) \\ 0 & 0 & 0 & 0 \\ 0 & 0 & 0 & 0 \\ I_1(ka_e) & I_1(k_2a_e) & K_1(ka_e) & K_1(k_2a_e) \\ kI_0(ka_e) & k_2I_0(k_2a_e) & -kK_0(ka_e) & -k_2K_0(k_2a_e) \\ F_5 & F_6 & F_7 & F_8 \\ G_5 & G_6 & G_7 & G_8 \end{bmatrix}. \tag{2.38}$$

Lengthy expressions for the functions F_i and G_i are given in Appendix A.† Setting the determinant of the matrix $\boldsymbol{M}$ equal to zero provides us with an algebraic, non-polynomial equation for the complex phase velocity c. Unfortunately, the number of solutions corresponding to distinct normal modes could not be assessed, except in the limit of Stokes flow, as will be discussed in § 3.

When the inner cylinder is absent, we obtain an annular layer surrounding a liquid thread. For small values of their arguments, the modified Bessel functions become singular, and the general expressions for the stream function (2.7) and (2.8) obtain singular terms. For the velocity to be regular at the x-axis, the constants $B_{1,1}$ and $B_{2,1}$ must be set equal to zero, and this yields the following simplified expressions for interior-fluid stream function:

$$\Psi_1 = \sigma(A_{1,1}I_1(k\sigma) + A_{2,1}I_1(k_1\sigma))\exp(\mathrm{i}k(x - ct)). \tag{2.39}$$

The linear system (2.36) undergoes analogous simplifications.

When the outer cylinder is absent, we obtain an annular layer coated on the exterior surface of a cylindrical tube surrounded by an outer infinite fluid. For large values of their arguments, the modified Bessel functions tend to become unbounded. To ensure a regular behaviour, we set the coefficients $A_{1,2}$ and $A_{2,2}$ equal to zero, and obtain the following simplified form for the exterior stream function:

$$\Psi_2 = \sigma(B_{1,2}K_1(k\sigma) + B_{2,2}K_1(k_2\sigma))\exp(\mathrm{i}k(x - ct)). \tag{2.40}$$

The linear system (2.36) undergoes analogous simplifications.

† Appendix A is available on request from the Journal of Fluid Mechanics Editorial Office or the author.

In the simplest configuration, both the internal and external cylinder are absent yielding an infinite thread suspended in an infinite ambient fluid. The stream functions for the internal and external flow are described, respectively, by equations (2.39) and (2.40). The linear system (2.36) undergoes analogous simplifications.

3. Linear stability analysis for Stokes flow

When inertial forces are negligible within both fluids, the modified wavenumbers k_j reduce to the wavenumber k, and equation (2.8) no longer provides us with the general solution. To study this limit, we expand the modified wavenumbers k_1 and k_2 in Taylor series about k with respect to the dimensionless phase velocities $\hat{c}_j = \mathrm{i}c/(kv_j)$ for $j = 1, 2$. Demanding that the resulting expression satisfies the equations of Stokes flow to first order with respect to $\hat{c}_j$, we derive Tomotika's (1936) expression

$$\begin{aligned}\Psi_j(\sigma) = \sigma \big(&C_{1,j} I_1(k\sigma) + D_{1,j} K_1(k\sigma) + C_{2,j} \tfrac{1}{2}\sigma(I_0(k\sigma) + I_2(k\sigma)) \\ &- D_{2,j} \tfrac{1}{2}\sigma(K_0(k\sigma) + K_2(k\sigma))\big) \exp(\mathrm{i}k(x - ct)),\end{aligned} \tag{3.1}$$

where $C_{l,j}$ and $D_{l,j}$ are new coefficients. In this case, we obtain the linear system (2.36), where the vector of unknowns is defined as

$$\boldsymbol{w} = [C_{1,1}, C_{2,1}, D_{1,1}, D_{2,1}, C_{1,2}, C_{2,2}, D_{1,2}, D_{2,2}] \tag{3.2}$$

and the coefficient matrix is given by

$$\boldsymbol{M} = \begin{vmatrix} I_1(ka) & H_1 & K_1(ka) & H_2 & -I_1(ka) & H_3 & -K_1(ka) & H_4 \\ kI_0(ka) & L_1 & -kK_0(ka) & L_2 & -kI_0(ka) & L_3 & kK_0(ka) & L_4 \\ I_1(ka_i) & N_1 & K_1(ka_i) & N_2 & 0 & 0 & 0 & 0 \\ kI_0(ka_i) & N_3 & -kK_0(ka_i) & N_4 & 0 & 0 & 0 & 0 \\ 0 & 0 & 0 & 0 & I_1(ka_e) & Q_1 & K_1(ka_e) & Q_2 \\ 0 & 0 & 0 & 0 & kI_0(ka_e) & Q_3 & -kK_0(ka_e) & Q_4 \\ S_1 & S_2 & S_3 & S_4 & S_5 & S_6 & S_7 & S_8 \\ T_1 & T_2 & T_3 & T_4 & T_5 & T_6 & T_7 & T_8 \end{vmatrix}. \tag{3.3}$$

Expression for the entries H_i, L_i, N_i, Q_i, S_i and T_i are given in Appendix B.† In the case of an internally bounded annular layer, an externally annular bounded, or an unbounded thread, the linear system (2.36) and the matrix (3.3) undergo straightforward simplifications, as discussed in the preceding section.

Alternatively, we may solve the following set of equations in place of (2.5):

$$\mathrm{D}^2\Psi_j^* = 0, \quad \mathrm{D}^2\Psi_j = \Psi_j^* \tag{3.4}$$

and work with the general solution

$$\Psi_j(\sigma) = \sigma(E_{1,j} I_1(k\sigma) + F_{1,j} K_1(k\sigma) + E_{2,j}\sigma I_0(k\sigma) + F_{2,j}\sigma K_0(k\sigma)) \exp(\mathrm{i}k(x - ct)) \tag{3.5}$$

derived by Goren (1962), where $E_{l,j}$ and $F_{l,j}$ are new coefficients. The properties of the Bessel functions ensure that expression (3.1) reduces to (3.5) by an appropriate grouping of the coefficients.

† Appendix B is available on request from the Journal of Fluid Mechanics Editorial Office or the author.

With the choice (3.5), we obtain the linear system (2.36), where the vector of unknowns is defined as

$$\boldsymbol{w} = [E_{1,1}, E_{2,1}, F_{1,1}, F_{2,1}, E_{1,2}, E_{2,2}, F_{1,2}, F_{2,2}] \tag{3.6}$$

and the coefficient matrix is given by

$$\boldsymbol{M} = \begin{vmatrix} I_1(ka) & aI_0(ka) & K_1(ka) & aK_0(ka) \\ kI_0(ka) & \hat{L}_1 & -kK_0(ka) & \hat{L}_2 \\ I_1(ka_i) & a_iI_0(ka_i) & K_1(ka_i) & a_iK_0(ka_i) \\ kI_0(ka_i) & \hat{N}_3 & -kK_0(ka_i) & \hat{N}_4 \\ 0 & 0 & 0 & 0 \\ 0 & 0 & 0 & 0 \\ S_1 & \hat{S}_2 & S_3 & \hat{S}_4 \\ T_1 & \hat{T}_2 & \hat{T}_3 & \hat{T}_4 \end{vmatrix}$$

$$\begin{vmatrix} -I_1(ka) & -aI_0(ka) & -K_1(ka) & -aK_0(ka) \\ -kI_0(ka) & \hat{L}_3 & kK_0(ka) & \hat{L}_4 \\ 0 & 0 & 0 & 0 \\ 0 & 0 & 0 & 0 \\ I_1(ka_e) & a_eI_0(ka_e) & K_1(ka_e) & a_eK_0(ka_e) \\ kI_0(ka_e) & \hat{Q}_3 & -kK_0(ka_e) & \hat{Q}_4 \\ S_5 & \hat{S}_6 & S_7 & \hat{S}_8 \\ T_5 & \hat{T}_6 & T_7 & \hat{T}_8 \end{vmatrix}. \tag{3.7}$$

Expressions for the entries $\hat{L}_i$, $\hat{N}_i$, $\hat{Q}_i$, $\hat{S}_i$, $\hat{T}_i$ are given in Appendix B. The second and sixth columns of (3.7) arise, respectively, by dividing the first and fifth columns of (3.3) by k, and adding the result to the second and sixth column, as shown in Appendix B. The fourth and eighth columns of (3.7) arise, respectively, by dividing the third and seventh columns of (3.3) by k, adding the result to the fourth and eighth columns, and then switching the sign of the resulting expressions, as shown in Appendix B.

Eliminating the denominators from all entries of matrix (3.3) or (3.7), by multiplying the corresponding rows by them, setting the determinant of the resulting matrix equal to zero, and simplifying the resulting expressions, we obtain a secular quadratic equation for the complex phase velocity c. This quadratic equation has two conjugate imaginary solutions corresponding to two normal modes with vanishing phase velocity. One of these modes is stable under any conditions, while the second one may be unstable when the reduced wavenumber ka is sufficiently small and the surface tension γ is sufficiently large compared to the modulus of elasticity E. In the absence of elastic tensions, the coefficient of the quadratic term in the secular equation vanishes, and we obtain a linear equation corresponding to a single normal mode, in agreement with well-known results for constant surface tension.

The occurrence of two normal modes in the presence of elastic tensions could have been predicted at the outset by the following arguments. An arbitrary axisymmetric monochromatic perturbation displaces material particles along the trace of the membrane in an azimuthal plane with waves of arbitrary amplitude and arbitrary phase

shift. A normal-mode perturbation requires a specific ratio between the axial and radial displacements, and a particular phase shift. Counting the number of unknowns involved in the decomposition of an arbitrary wave into normal modes reveals that only two such modes are necessary. In the absence of elastic tensions, the displacement of the material particles is relevant only insofar as it determines the shape of the perturbed interface, and one of the normal modes disappears, as will be described later in this section. One might argue that similar arguments can be made for the more general case of Navier–Stokes flow, but the generalization is not appropriate: only in Stokes flow does specifying the interfacial geometry and distribution of boundary velocity and interfacial traction uniquely determine the flow.

We proceed now to present and discuss stability graphs for several cases that illustrate the effect of the ratio of the membrane tension to the modulus of elasticity γ/E, viscosity ratio $\lambda = \mu_2/\mu_1$, and reduced cylinder radii a_i/a and a/a_e.

First, we consider a thread suspended in an infinte ambient fluid, in the absence of an internal or external cylinder. In figure 3(*a*), we plot the dimensionless growth rate $\hat{\sigma}_I \equiv \mu k c_I a/(\gamma + E)$ against the reduced wavenumber ka, for $\lambda = 1$, and $\gamma/E = 0.001$, 0.1, 0.5, 1, 2, 5, 10, 20; c_I is the imaginary part of the complex phase velocity. The dashed lines correspond to the conditionally unstable normal mode, and the solid lines correspond to the stable normal mode. It is clear from these graphs that the elastic tensions dampen the instability due to surface tension. Considering the conditionally unstable normal mode, we note that as the ratio γ/E is reduced, the range of unstable wavenumber ka shrinks from $(0, 1)$ to $(0, ka_{stb})$, where ka_{stb} is a critical value. In the limit as γ/E tends to zero, the threshold ka_{stb} tends to zero indicating that elastic tensions, however large, are unable to stabilize disturbances with sufficiently small wavenumbers. The growth rate of the unstable modes, however, is drastically reduced in this limit, and for all practical purposes the instability may be regarded as being suppressed below a certain threshold.

It is illuminating to consider in some detail the properties of the normal modes for the thread discussed in the preceding paragraph. In figure 3(*b*), we plot the ratio of the axial to radial displacement of material points along the interface, δ, defined in equation (2.35), against the reduced wavenumber, on a linear-log scale. The singularities in the dashed lines correspond to a change in the sign of δ from negative values on the left, to positive values on the right. In all cases, as the wavenumber tends to zero, the magnitude of δ tends to infinity, and this indicates that the radial displacement of point particles along the membrane tends to become very small compared to the axial displacement. That is, the normal modes correspond to in-plane deformation of the membrane yielding compression waves. At the wavenumbers where the dashed lines exhibit singularities, the converse is true: the axial displacement of point particles vanishes, and the normal modes denote peristaltic waves. As γ/E becomes smaller, the wavenumbers where sign inversion occurs are shifted to larger values and eventually to infinity. As the ratio γ/E is raised, the displacement ratio δ corresponding to the dashed lines for wavenumbers that are larger than the critical one for sign inversion obtain increasingly larger values corresponding to small radial displacements. A similar behaviour is exhibited by the solid lines for wavenumbers that are smaller than the critical wavenumber. These asymptotic behaviours are responsible for the disappearance of one of the normal modes in the limit of vanishing elastic tensions.

To illustrate the effect of the viscosity ratio, in figure 4(*a*) we present results that are analogous to those shown in figure 3(*a*), but for viscosity ratio $\lambda = 0$ corresponding to a viscous thread suspended in an inviscid ambient fluid. The behaviour of the growth

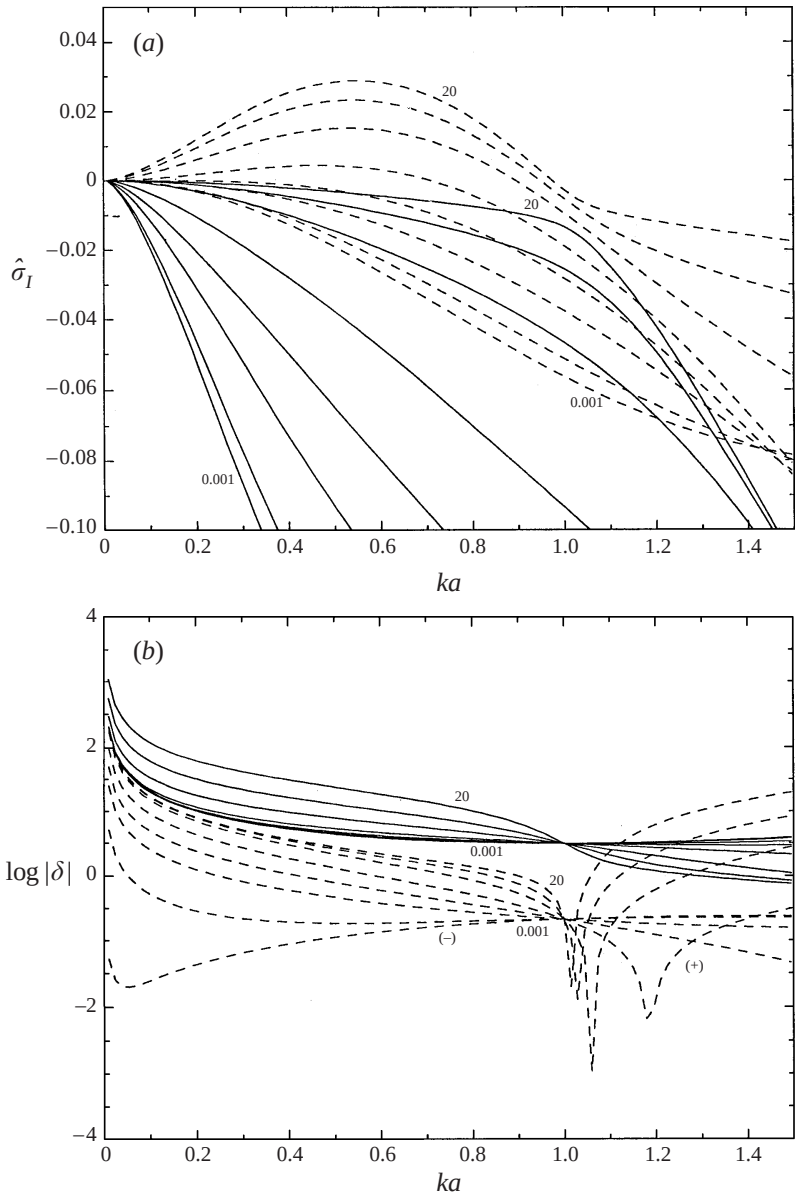

FIGURE 3. (*a*) The dimensionless growth rate $\hat{\sigma}_I \equiv \mu k c_I a/(\gamma + E)$ vs. the reduced wavenumber ka, for $\lambda = 1$, and $\gamma/E = 0.001$, 0.1, 0.5, 1, 2, 5, 10, 20; c_I is the imaginary part of the complex phase velocity. The dashed lines correspond to the conditionally unstable normal mode, and the solid lines correspond to the stable normal mode. (*b*) Corresponding graphs of the ratio δ between the axial to radial displacement of material points along the interface, defined in equation (2.35).

rate and displacement amplitude ratio is similar to that for $\lambda = 1$, with one important exception: in the limit of vanishing wavenumbers, the growth rate does not vanish, but tends to a non-zero value that depends on the ratio γ/E. This behaviour has been noted and discussed previously for interfaces with constant or variable surface tension

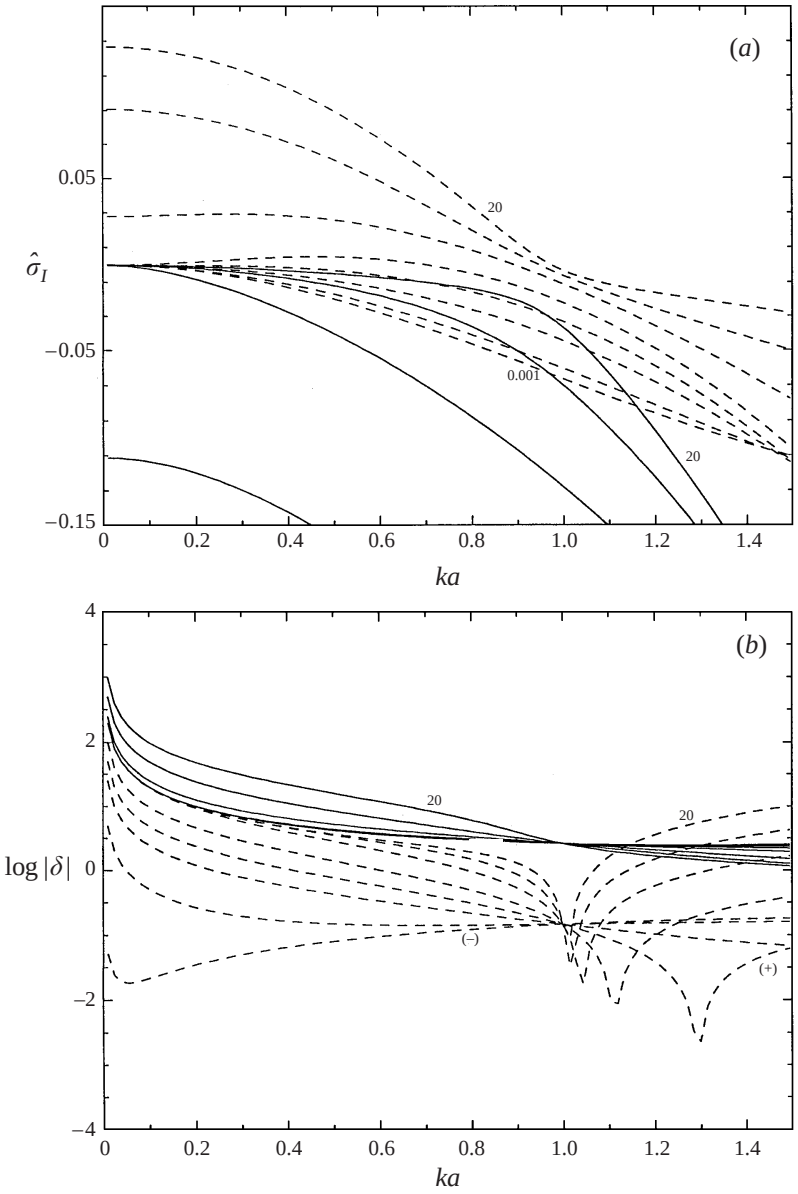

FIGURE 4. As figure 3 but for a viscous thread suspended in an inviscid medium, corresponding to $\lambda = 0$.

(e.g. Pozrikidis 1999; Kwak & Pozrikidis 1999). The behaviour of the displacement ratio is shown in figure 4(*b*).

Next, we discuss the influence of the internal and external cylinders on the growth rates and on the properties of the normal modes. In figure 5(*a*, *b*), we present graphs of the reduced growth rate and displacement ratio δ of the two normal modes, for a core–annular arrangement – that is in the absence of the inner cylinder but in the presence of an outer cylinder – for $\lambda = 1$, $\gamma/E = 5$, and for $a_e/a = 1.2, 1.5, 2, 3, 4, 5, 10, \infty$. Figure 5(*a*) reveals a significant reduction in the growth rate of the conditionally

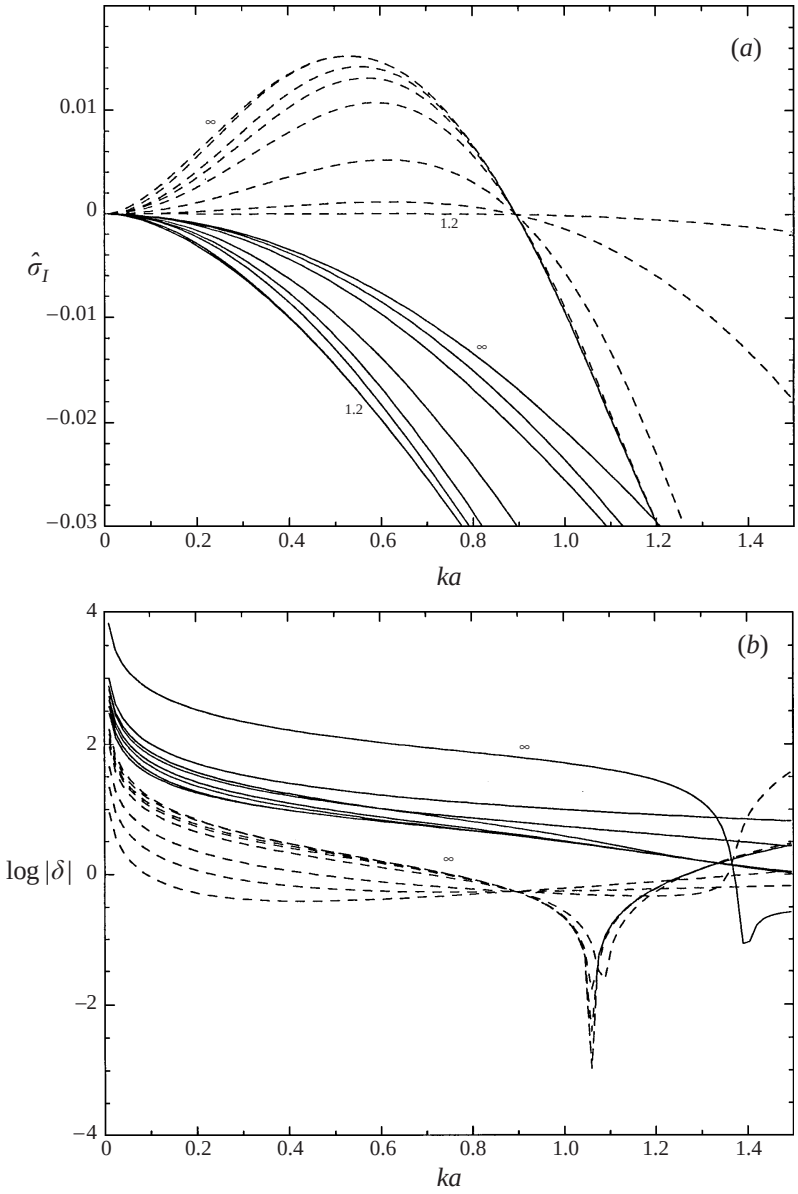

FIGURE 5. Effect of an outer cylinder on the stability of a thread: (*a*) the dimensionless growth rate and (*b*) displacement ratio, for $\lambda = 1$, $\gamma/E = 5$, and $a_e/a = 1.2, 1.5, 2, 3, 4, 5, 10, \infty$.

unstable mode as the outer cylinder approaches the interface, accompanied by a noticeable shifting of the wavenumber for maximum growth toward higher values. The negative growth rate of the stable mode is less sensitive to the presence of the outer cylinder. The corresponding behaviour of δ is illustrated in figure 5(*b*), showing that the presence of the cylindrical boundary may cause an inversion in the sign of δ.

In figure 6, we present analogous results for an annular film coated on the exterior

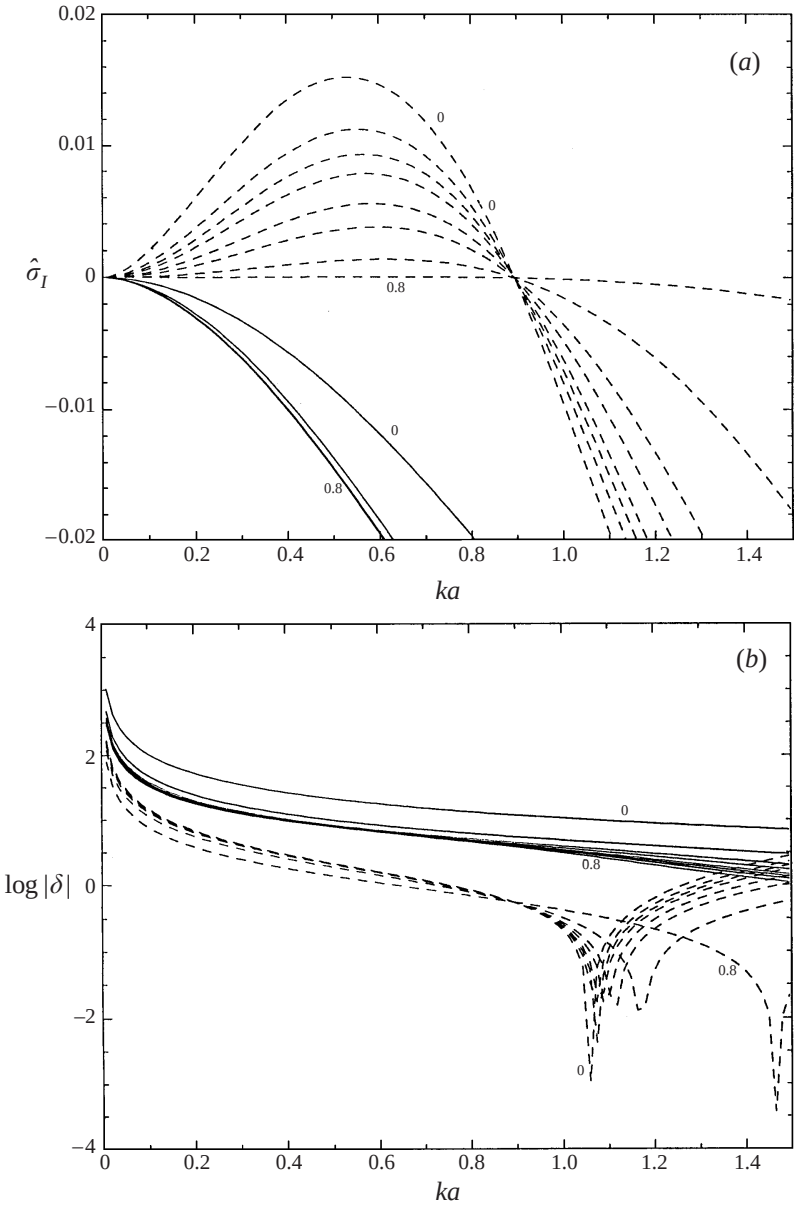

FIGURE 6. Effect of an inner cylinder in the stability of an annular layer: (*a*) the dimensionless growth rate and (*b*) displacement ratio, for $\lambda = 1$, $\gamma/E = 5$, and $a_i/a = 0$, 0.01, 0.05, 0.1, 0.2, 0.3, 0.5, 0.8.

surface of a tube – that is in the presence of an inner cylinder but in the absence of an outer cylinder – for $\lambda = 1$, $\gamma/E = 5$, and for $a_i/a = 0$, 0.01, 0.05, 0.1, 0.2, 0.3, 0.5, 0.8. The behaviour of the growth rate and of the displacement amplitude ratio are qualitatively similar to those described in the previous paragraph. It is striking to note that the presence of an inner cylinder whose radius is only 1% of the radius of the thread reduces by approximately 20% the growth rate of both normal modes.

4. Nonlinear instability of a thread in Stokes flow

In the second part of this paper, we study the nonlinear stages of the instability of an infinite thread, in the absence of an internal or external cylinder, in the limit of vanishing Reynolds number. These studies are based on numerical solutions of the equations of Stokes flow using a boundary integral method. The main goal is to examine whether and how the development of elastic tensions due to large interfacial deformations restricts the growth of unstable waves and leads to stationary axisymmetric waves similar to those observed in the experiments discussed in the introduction. In § 4.1 we present the numerical method, and in § 4.2 we discuss the results of the simulations.

4.1. *Numerical method*

Consider an infinite, periodic, axisymmetric thread of a fluid of equivalent radius a and viscosity μ, suspended in an ambient fluid with viscosity $\lambda\mu$, with the interface exhibiting evolving axisymmetric undulations of wavelength L. Following a well-established formalism (e.g. Pozrikidis 1992), we derive the following Fredholm integral equation of the second kind for the interfacial velocity:

$$u_\alpha(\boldsymbol{x}_0) = -\frac{1}{4\pi\mu(1+\lambda)} \int_C G_{\alpha\beta}(\boldsymbol{x}_0, \boldsymbol{x}) \Delta f_\beta(\boldsymbol{x}) \, \mathrm{d}l(\boldsymbol{x}) + \frac{1-\lambda}{1+\lambda} \frac{1}{4\pi} \int_C^{\mathrm{PV}} Q_{\alpha\beta\gamma}(\boldsymbol{x}_0, \boldsymbol{x}) u_\beta(\boldsymbol{x}) n_\gamma(\boldsymbol{x}) \, \mathrm{d}l(\boldsymbol{x}), \tag{4.1}$$

where the point $\boldsymbol{x}_0$ lies at the interface, and the rest of the symbols are defined as follows: Greek subscripts stand for the axial and radial polar cylindrical coordinates x or σ, C is one period of the contour of the interface in an azimuthal plane; l is the arclength along C; $\boldsymbol{n}$ is the unit vector normal to the interface pointing into the thread; PV denotes the principal value of the double-layer potential expressed by the second integral on the right-hand side of (4.1). The kernels $\boldsymbol{G}$ and $\boldsymbol{Q}$ are the periodic Green's functions of axisymmetric Stokes flow for the velocity and stress, where the wavelength of the flow associated with the Green's function matches that of the flow under consideration. The computation of $\boldsymbol{G}$ and $\boldsymbol{Q}$ in terms of expedited sums, the properties of the integral equation (4.1), and numerical method for solving the integral equation are discussed by Pozrikidis (1999).

The jump in the traction across the interface $\Delta\boldsymbol{f}$ involved in the single-layer potential expressed by the first integral on the right-hand side of (4.1), is given in equations (2.17) and (2.18). We consider neo-Hookean membranes consisting of a thin layer of an incompressible elastic material that obeys the linear version of Mooney constitutive law, and write

$$\tau_{ll} = \frac{E}{3} \frac{1}{\lambda_l \lambda_\varphi} \left(\lambda_l^2 - \frac{1}{\lambda_l^2 \lambda_\varphi^2} \right) \tag{4.2}$$

and

$$\tau_{\varphi\varphi} = \frac{E}{3} \frac{1}{\lambda_l \lambda_\varphi} \left(\lambda_\varphi^2 - \frac{1}{\lambda_l^2 \lambda_\varphi^2} \right), \tag{4.3}$$

where E is Young's modulus of elasticity (Li *et al.* 1988; McDonald 1996). In the limit of small deformations, equations (4.2) and (4.3) yield the linearized forms (2.25).

To describe the motion of the interface, we trace one period of it in an azimuthal plane with a set of point particles, approximate the contour of the interface by a

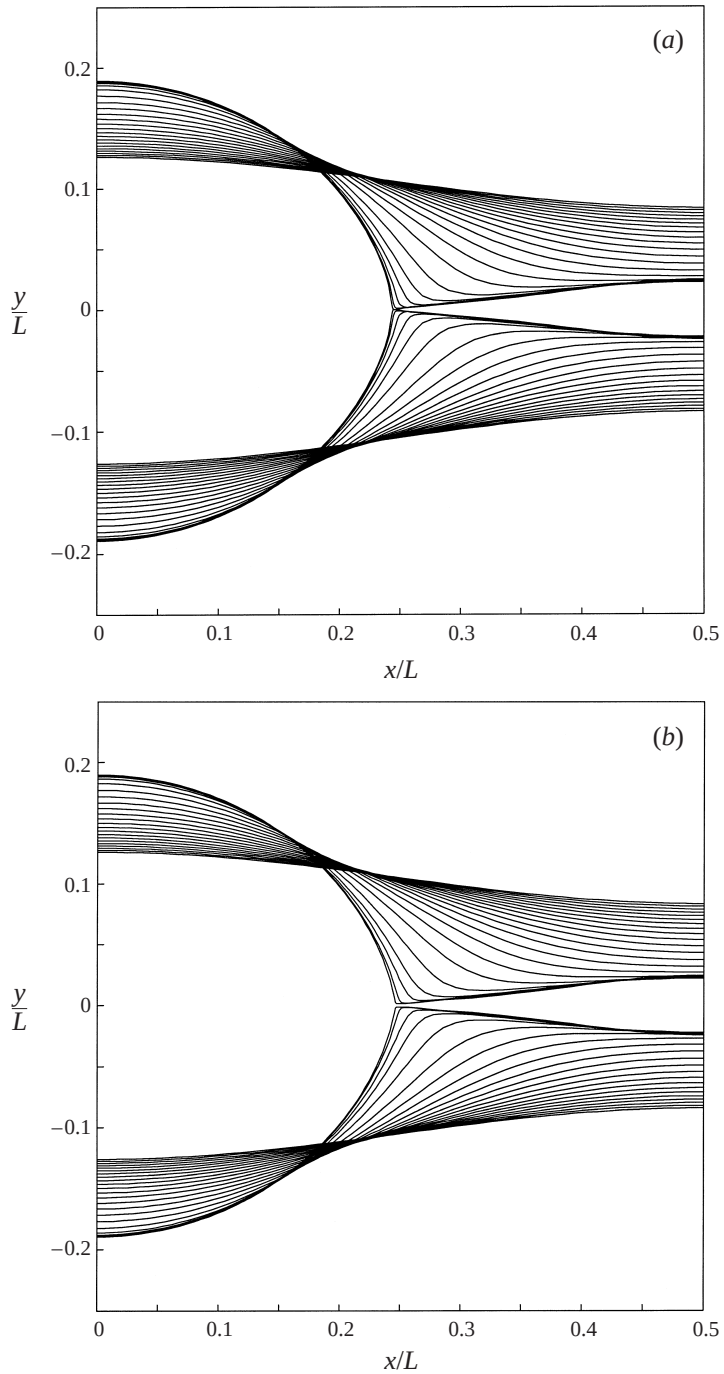

FIGURE 7. Stages in the instability of a thread for $\lambda = 1$, in the absence of interfacial elasticity, $E = 0$, subject to a sinusoidal perturbation with reduced wavenumber $ka = \frac{2}{3}$ and amplitude $a_1/a = 0.20$. (*a*) Results obtained without smoothing, and (*b*) results obtained with smoothing the position of the marker points. The profiles shown correspond to time intervals of $2.5\,\mu a/\gamma$.

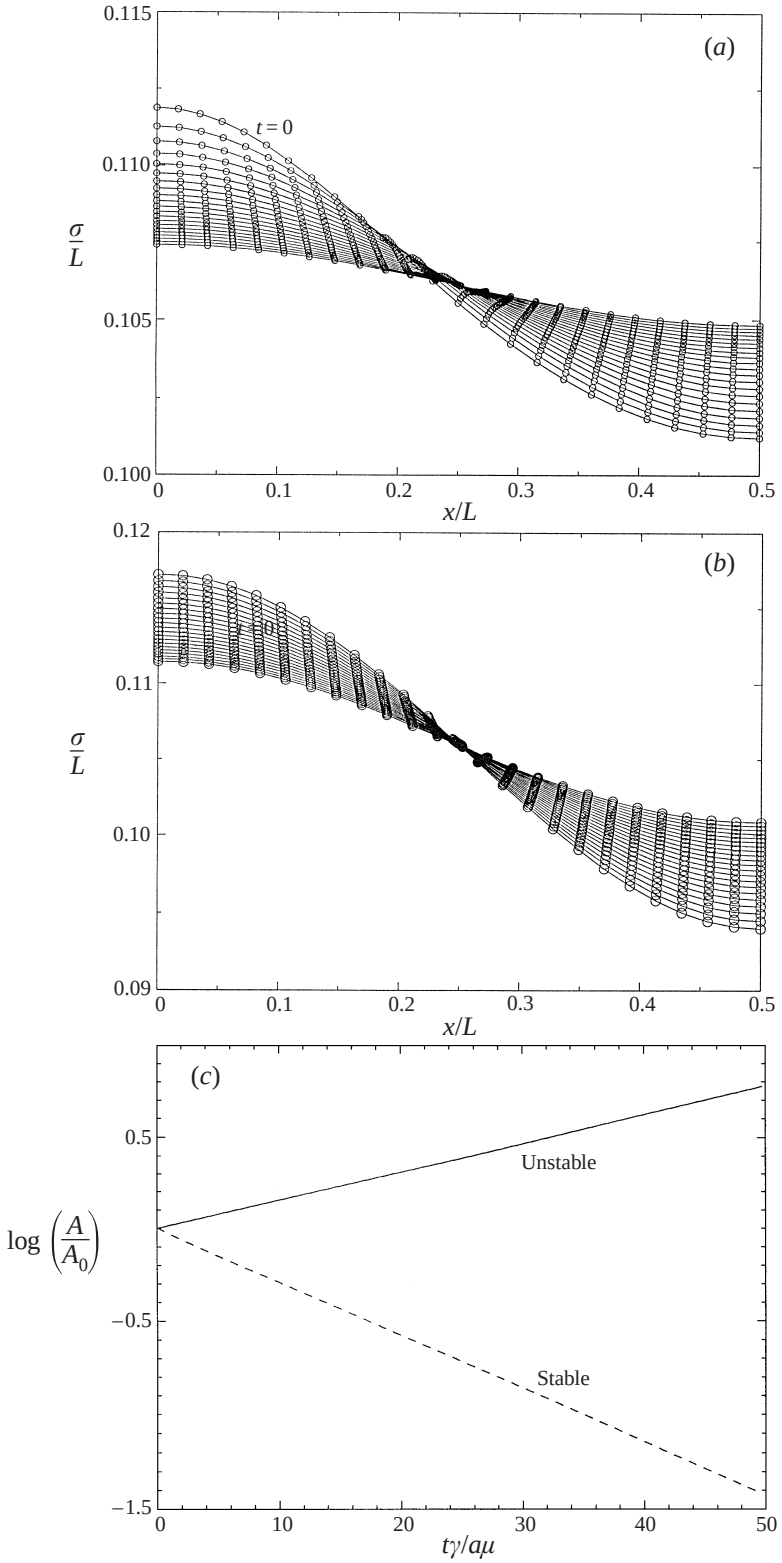

FIGURE 8. For caption see facing page.

collection of blended circular arcs, solve the integral equation (4.1) for the velocity using a boundary-element method, and advance the position of the point particles using the first- or second-order Runge–Kutta method. In the numerical implementation, the jump in traction and interfacial velocity are assumed to vary linearly over the boundary elements with respect to arclength. Implementing this approximation yields a system of linear equations for the velocity at the nodes that is solved by the method of Gauss elimination. When $\lambda = 1$, the coefficient of the second integral on the right-hand side of (4.1), termed the Stokes double-layer potential vanishes, leaving an integral representation in terms of the first integral alone, termed the Stokes single-layer potential. All derivatives required for the computation of $\Delta \boldsymbol{f}$ are evaluated using second-order centred differences.

In the course of a simulation, marker points are added at regions of large curvature, or when two adjacent marker points have been separated by a large distance due to stretching. The position of the new points at the unstressed state, necessary for the computation of the elastic tensions, is evaluated by quadratic interpolation with respect to arclength. Points are removed when clustering occurs at regions of low curvature, but only when the resulting distribution does not violate the aforementioned two constraints. A typical simulation begins with 64 marker points and ends with 120 marker points. Numerical error causes the volume of the thread over a period to decrease slightly during the simulations. The change is less than 0.5% in all cases, and less that 0.1% in most cases. A typical simulation with $\lambda = 1$ requires approximately 30 hours of CPU time, and a simulation with $\lambda \neq 1$ requires approximately 60 hours of CPU time on a SUN SPARCstation 20.

Interfacial elasticity causes numerical instabilities similar to, but more severe than, those reported by Li *et al.* (1988) for axisymmetric capsules deforming under the action of a uniaxial extensional flow. In the case of a thread, portions of the interface undergo compression that causes wrinkling in the absence of bending moments. The instabilities may be suppressed by raising the number of marker points while decreasing the size of the time step, but exorbitant demands on computational time place a pragmatic restriction on the method. As an alternative, we follow Li *et al.* (1988) and smooth the Cartesian coordinates of the marker points using the five-point formula of Longuet-Higgins & Cokelet (1976) which amounts to allowing the coordinates of the marker points to undergo numerical diffusion. In certain cases, we also smooth the distribution of the elastic tensions and components of the traction discontinuity $\Delta \boldsymbol{f}$ just before the evaluation of the single-layer potential, but this smoothing is not critical for the viability of the simulations; performing the single-layer integral smooths out irregularities in the distribution of elastic tensions and of $\Delta \boldsymbol{f}$ and yields a less irregular velocity.

To investigate the effect of smoothing on the physical relevance of the results, we performed a number of exploratory studies. Figure 7 shows stages in the instability of a thread with $\lambda = 1$, in the absence of interfacial elasticity, $E = 0$, subject to a sinusoidal perturbation with wavenumber $ka = \frac{2}{3}$ and amplitude $0.20a$. Figure 7(*a*) shows results obtained without smoothing, and figure 7(*b*) shows corresponding results

FIGURE 8. Successive stages in the evolution of a thread with $\lambda = 1$ and $\gamma/E = 5$, subject to a normal-mode perturbation with reduced wavenumber $ka = \frac{2}{3}$ and amplitude $\eta/a = 0.05$; (*a*) stable normal-mode perturbation, and (*b*) unstable perturbation. The profiles shown correspond to time intervals of $2.5\,\mu a/\gamma$. (*c*) Evolution of the reduced amplitude of the interfacial wave for the stable mode (dashed line), and for the unstable mode (solid line), showing excellent agreement with the predictions of linear stability theory.

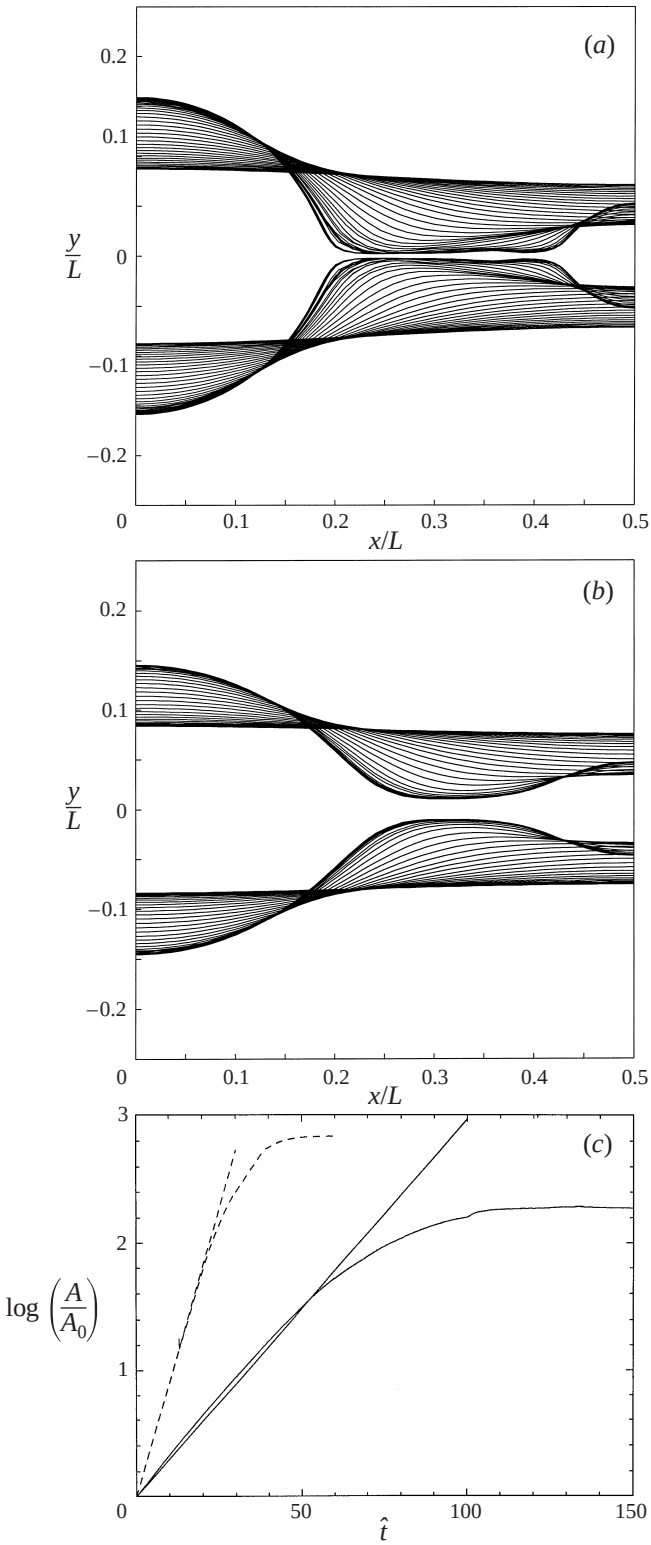

FIGURE 9. For caption see facing page.

obtained with smoothing the position of the marker points at every time step. In both cases, the sinusoidal waves amplify at a rate that is in excellent agreement with the predictions of linear theory, and the thread pinches off at a finite time near the base of the developing drops. Observable differences arise only at the late stages of breakup; smoothing, however, does not prevent pinching at the apex of the developing double cone. These and other exploratory simulations suggest that smoothing does not affect drastically the main features of the interfacial motion.

4.2. *Numerical simulations*

At the initial instant, point particles along the trace of the membrane in an azimuthal plane are displaced so that their coordinates are given by

$$X = x_U + \eta \sin(kx_U), \quad \Sigma = a + \xi \cos(kx_U), \tag{4.4}$$

where x_U is the axial position in the unstressed state corresponding to the cylindrical interface. A normal-mode perturbation requires that the displacement amplitudes η and ξ be small compared to the thread radius a, and the ratio η/ξ take the specific value δ defined in equation (2.15).

First, we confirm that the results of the simulations are consistent with the predictions of linear stability theory in the limit of small deformations. Figure 8(a,b) displays successive stages in the evolution of a thread with $\lambda = 1$, $\gamma/E = 5$, subject to a perturbation with wavenumber $ka = \frac{2}{3}$ and amplitude $\eta/a = 0.05$. The depicted profiles correspond to evenly spaced time intervals from the initial instant up to time $50\,\mu a/\gamma$. Figure 8(a) corresponds to a stable normal mode with $\xi/a = -0.293$, and figure 8(b) corresponds to an unstable normal mode with $\xi/a = -0.0668$. Figure 8(c) displays the evolution of the reduced amplitude of the interfacial wave for the stable and unstable mode, drawn with the dashed and solid line, respectively, on a linear-logarithmic scale; A is half the difference between the maximum and minimum radial position of the interface, and A_0 is the amplitude at the initial instant. In both cases, we obtain straight lines whose slopes are virtually identical to those predicted by linear stability theory, respectively, equal to -0.0280 and 0.0157.

We proceed next to examine the effect of the interfacial elasticity, considering first fluids with equal viscosity, $\lambda = 1$, and a perturbation with wavenumber $ka = 0.5$. In the absence of surface elasticity, the evolution of the thread is similar to that depicted in figure 7, leading to the development of a double cone that pinches off at a finite time to yield a series of disconnected drops (Pozrikidis 1999). Figure 9(a) displays stages in the evolution of the thread for an interface with a small modulus of elasticity, $E/\gamma = 0.05$, and for a perturbation with axial and radial displacement amplitudes $\eta/a = 0.10$, and $\xi/a = -0.0068$; these conditions do not correspond to a normal mode. Small-scale instabilities due to inadequate spatial resolution prevented the continuation of the simulation beyond the last profile shown. Figure 9(b) displays stages in the evolution of a thread with a larger modulus of elasticity, $E/\gamma = 0.20$, for a perturbation with displacement amplitudes $\eta/a = 0.05$, and $\xi/a = -0.10935$; these conditions do correspond to a normal mode. In both cases, the interfacial waves grow in agreement with the predictions of linear theory. As, however, the minimum thread

FIGURE 9. Successive stages in the instability of a thread for $\lambda = 1$ subject to a perturbation with reduced wavenumber $ka = 0.5$, for (a) $E/\gamma = 0.05$, $\eta/a = 0.10$, and $\xi/a = -0.0068$; the profiles shown correspond to time intervals of $4\,\mu a/\gamma$, (b) $E/\gamma = 0.20$, $\eta/a = 0.05$, and $\xi/a = -0.10935$; the profiles shown correspond to time intervals of $10\,\mu a/\gamma$. (c) The evolution of the reduced amplitude of the perturbation; the straight lines represent the prediction of the linear stability theory.

radius reaches a certain value, the growth is arrested yielding slowly evolving shapes consisting of alternating sequences of primary drops and secondary drops connected by elongated ligaments.

Figure 9(c) displays the evolution of the reduced amplitude of the interfacial wave. The straight lines represent the predictions of the linear theory for the unstable normal mode shown in figure 3(a). The dashed lines corresponds to figure 9(a), and the dimensionless time is defined as $\hat{t} = t\gamma/a\mu$; the solid lines corresponds to figure 9(b), and the dimensionless time is defined as $\hat{t} = tE/a\mu$. At small times, the numerical results are in good or excellent agreement with the predictions of the linear theory, even though the amplitude of the perturbation is not small or the initial condition may not correspond to a normal mode. The saturation of the instability is evidenced by the levelling of the growth curves at long times.

Figure 10(a, b) shows the distribution of the elastic tensions over half a period of the final profile shown in figure 9(a, b); the solid lines correspond to τ_{ll}, and the dashed lines correspond to $\tau_{\varphi\varphi}$. Both tensions take small or moderate values over the primary and secondary bulges, and pronounced values over the connecting links. For both cases illustrated in figure 10, the minimum value of is $\tau_{\varphi\varphi}$ is on the order of $-\gamma$, and this suggests that the instability reaches equilibrium when the sum of the elastic tension in the azimuthal direction and the surface tension has become sufficiently small. This observation provides us with criterion for estimating the minimum thread radius at equilibrium on the basis of the constitutive equations (4.4). Near the regions of minimum thread radius of a substantially deformed interface, the radial stretch ratio λ_φ is smaller than the azimuthal stretch ratio λ_l. To leading order, equation (4.3) produces the negative elastic tension

$$\tau_{\varphi\varphi} \approx -\frac{E}{3}\frac{1}{\lambda_l^3\lambda_\varphi^3}. \tag{4.5}$$

Equating the magnitude of this tension to the surface tension γ produces the following estimate for the minimum thread radius at equilibrium:

$$\sigma_{Min} \approx a\frac{1}{\lambda_l}\left(\frac{1}{3}\frac{E}{\gamma}\right)^{1/3}. \tag{4.6}$$

The numerical results show that, for the evolution shown in figure 9(b), the maximum value of λ_l over the narrow bridge is on order 3, yielding the estimate $\sigma_{Min}/L \approx 0.022$ which is in good agreement with the results of the simulation. For the evolution shown in figure 9(a), the corresponding estimate is $\sigma_{Min}/L \approx 0.01$.

The results presented in figure 9 suggest that the thread evolves toward an equilibrium configuration with a deformed interfacial shape. If perfect equilibrium were established, the fluids on either side of the interface would be stationary, and the pressure inside the thread would be uniform. In figure 11(a, b), we plot the distribution of the tangential and normal components of the jump in traction across the interface corresponding to the final profile shown in figure 9(a, b); the tangential component is drawn with a solid line, and the normal component is drawn with a dashed line. In the absence of fluid motion, the tangential component must vanish and the normal component must be equal to the uniform pressure jump across the interface. Figure 11 shows that the tangential component fluctuates around zero mainly due to numerical error, whereas the normal component undergoes a substantial oscillation as it stretches between two uniform values prevailing at the beginning and near the mid-point of each period. This variation indicates that equilibrium has not been yet

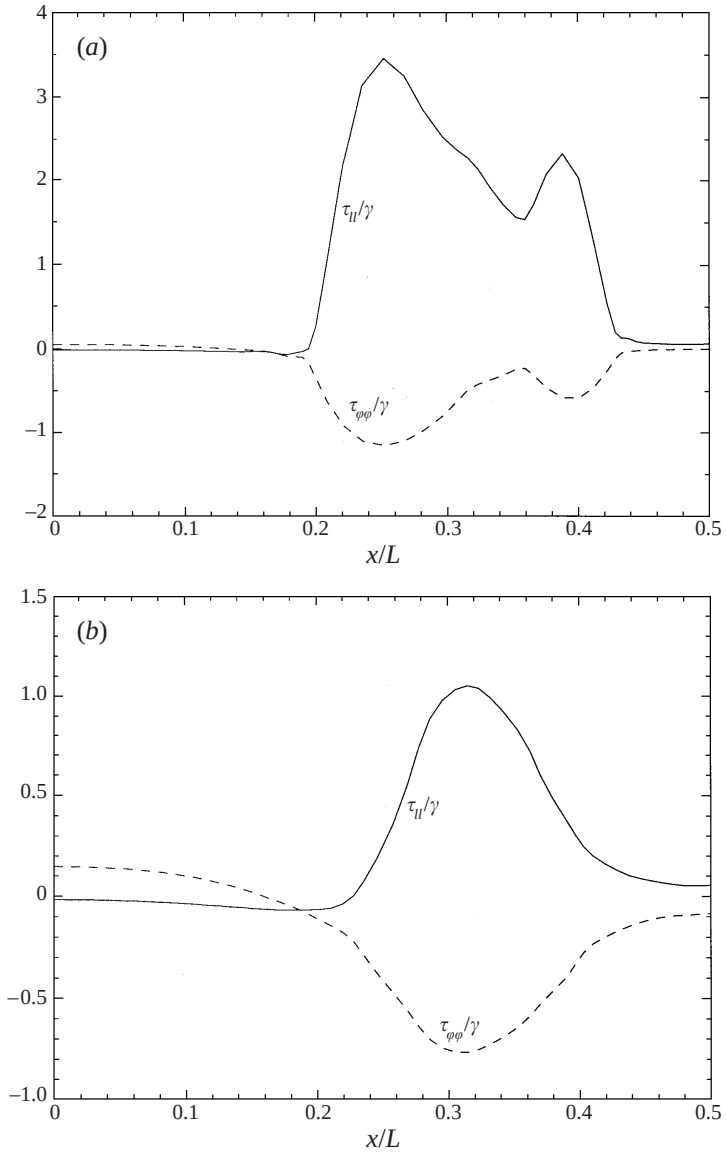

FIGURE 10. Distribution of the elastic tensions along the interface corresponding to the final profile shown in figure 9(*a*, *b*).

established, but the intensity of the flow driven by the pressure gradient is small due to the small radius of the ligaments connecting the bulges.

Next, we consider the evolution of a thread suspended in an inviscid ambient fluid corresponding to the viscosity ratio $\lambda = 0$. Figure 12(*a*) displays stages in the evolution of the thread for a perturbation with wavenumber $ka = 0.5$ and vanishing surface elasticity, showing continuous thinning at the trough of the perturbation followed by breakup at a finite time. In an earlier study (Pozrikidis 1999), it was shown that the process of thinning is captured by a similarity solution discovered by Papageorgiou (1995). It is important to note that the thread breaks up at the troughs only in the two limiting cases $\lambda = 0$ or ∞; at intermediate values, breakup occurs asymmetrically, as

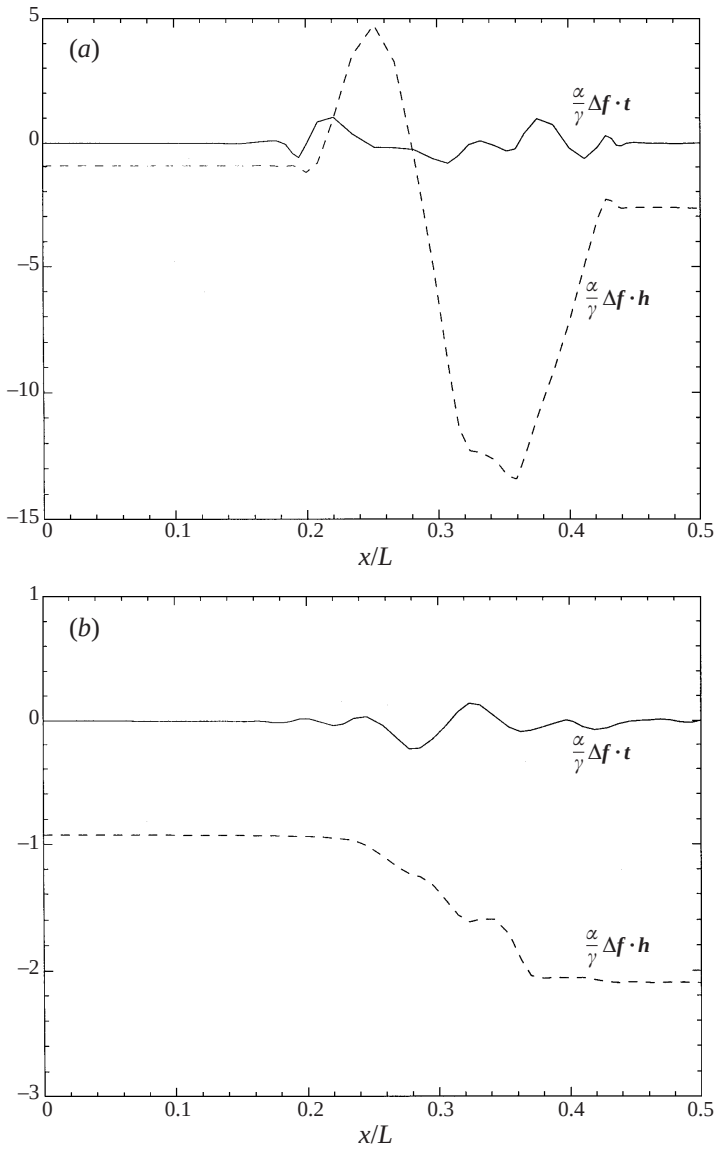

FIGURE 11. Distribution of the tangential and normal components of the jump in traction across the interface corresponding to the final profile shown in figure 9(*a*, *b*).

depicted in figure 7 for $\lambda = 1$. Figure 12(*b*, *c*) displays typical stages in the evolution of a thread with $E/\gamma = 0.05$, 0.20, subject to a perturbation with $ka = 0.5$, and with initial conditions corresponding to the unstable normal mode. In both cases, the initial growth rate of the perturbation is in excellent agreement with the predictions of the linear stability theory presented in figure 4(*b*). It is striking to observe that even a small amount of elasticity is able to shift the point of minimum thread radius from the mid-point of a wavelength to an off-centred position yielding bulged shapes.

The numerical results indicate that, in the presence of surface elasticity, a thread with $\lambda = 0$ tends to an equilibrium shape with a quiescent internal fluid. In figure 13(*a*), we plot the distributions of the elastic tensions corresponding to the final profile shown

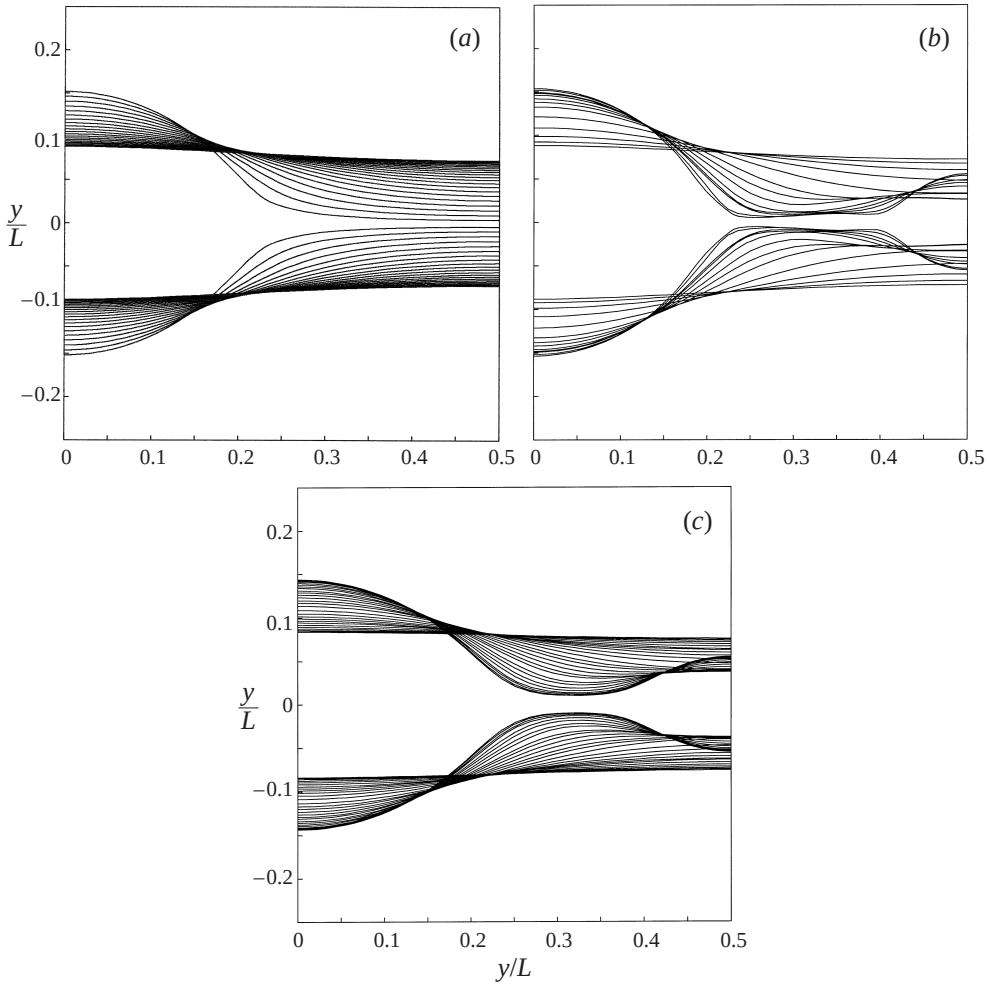

FIGURE 12. Typical stages in the instability of a thread for $\lambda = 0$, $ka = 0.5$ and (*a*) $E/\gamma = 0$ (the profiles shown correspond to time intervals of $0.5\,\mu a/\gamma$), (*b*) $E/\gamma = 0.05$ (corresponding to time intervals of $5\,\mu a/\gamma$), and (*c*) $E/\gamma = 0.20$ (Corresponding to time intervals of $7.5\,\mu a/\gamma$). The initial condition corresponds to the unstable normal mode.

in figure 12(*c*), and compare them to those shown in figure 10(*b*) to find reasonable agreement. In figure 13(*b*), we plot the profile of the interface at the end of the simulation with $\lambda = 1$ (solid line) or 0 (dashed line). Considering that the flow is still evolving, albeit at a slow rate, we find reasonable agreement. Similar results were obtained for $E/\gamma = 0.05$, although the agreement was less satisfactory due to the limited duration of the simulation. The need to use a moderate number of marker points in order to suppress numerical instabilities undermines the effectiveness of the numerical method for thin cross-sections.

5. Concluding remarks

We have studied the linear stability of a cylindrical interface that exhibits constant surface tension and develops elastic tensions due to the deformation, subject to axisymmetric perturbations. The results confirmed that elastic tensions stabi-

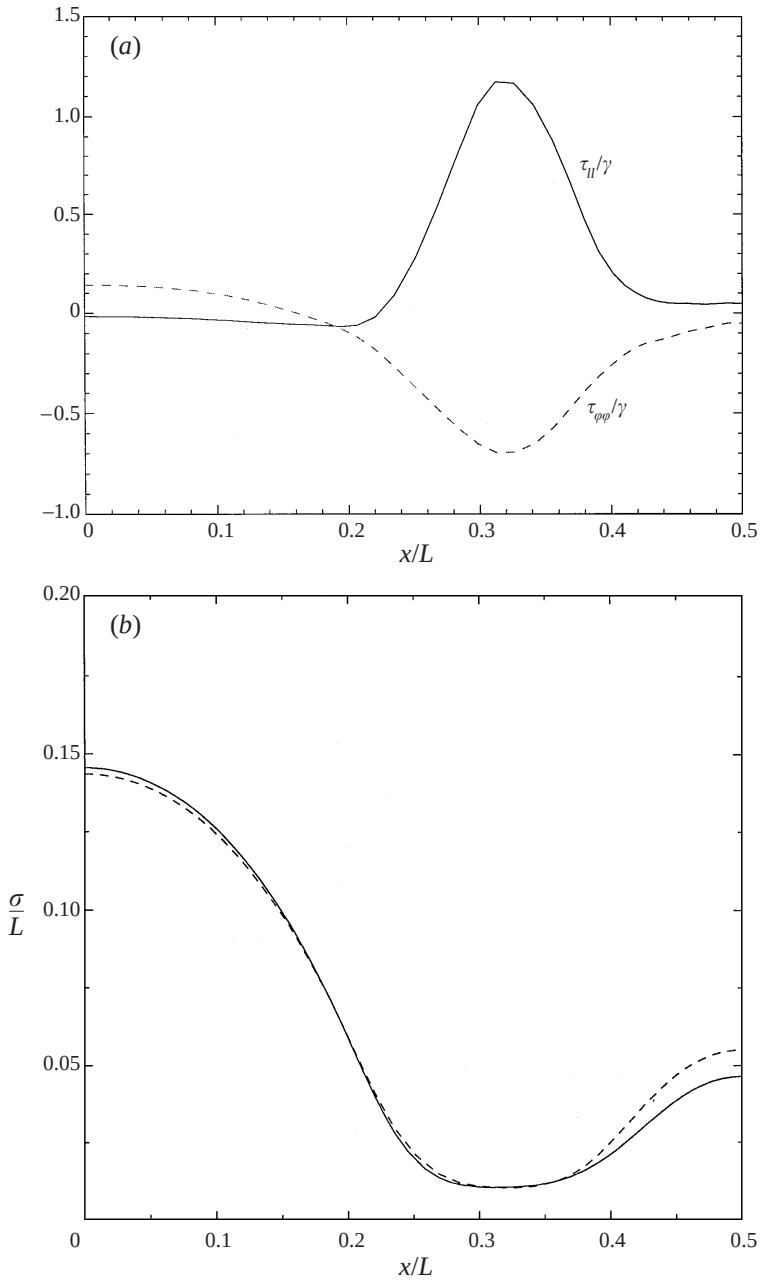

FIGURE 13. (*a*) Distributions of the elastic tensions corresponding to the final profile shown in figure 12(*c*). (*b*) Comparison of the interface profile at the end of the simulation with $\lambda = 1$ (solid line) or 0 (dashed line).

lize perturbations of sufficiently small wavelength that would have been unstable if elastic tensions did not develop. Perturbations of sufficiently large wavelength, however, remain unstable, and the thread is overall conditionally stable. In practice, the largest wavelength allowed is determined by the size of the physical system that supports the thread at its ends, and the stability cut-off is determined by

the length of the thread as well as by the conditions prevailing at the support points.

Kwak & Pozrikidis (1999) studied the effect of an immiscible surfactant on the instability of an annular layer or an infinite thread, and confirmed that the presence of the surfactant reduces the growth of the perturbations but does not affect the range of unstable reduced wavenumbers ka; a is the thread radius. The unstable range is confined between zero and unity irrespective of the presence of the inner or outer cylinder. In contrast, elastic tensions not only reduce the magnitude of the growth rate, but also diminish the range of unstable wavenumbers.

There are certain similarities between the instability of the infinite thread considered here, and the instability of partially or totally liquid-filled elastic tube containing a stationary or moving fluid, as discussed in the introduction (e.g. Pedley & Luo 1998; Heil 1997, 1998). When the magnitude of a negative transmural pressure is sufficiently large, the tube has been observed to buckle into a non-axisymmetric shape, which indicates that the system becomes unstable to non-axisymmetric perturbations. In contrast, the Rayleigh instability of a cylindrical interface with constant surface tension, corresponding to a positive transmural pressure, favours axisymmetric perturbations. This comparison supports the conjecture that the sign of the transmural pressure determines the geometrical nature of the most dangerous mode.

The numerical results discussed in § 4 suggest the existence of a two-parameter family of stable equilibrium shapes determined by the reduced elasticity E/γ and the reduced wavenumber ka, in the range of wavenumbers where the thread is linearly unstable, independent of the viscosity ratio. These equilibrium shapes may be computed directly based on the membrane equilibrium equations with an *a priori* unknown constant pressure drop across the interface. For a specified non-zero value of the ratio E/γ, a family of stationary and stable shapes is expected to emanate from the critical wavenumber ka for neutral stability; another obvious family of unstable stationary shapes corresponds to the unperturbed cylindrical thread with an associated pressure jump across the interface equal to γ/a. In the absence of bending moments, the distribution of elastic stresses along the deformed shapes will be non-singular provided that the membrane does not become perpendicular to the axis at any point. Zarda *et al.* (1977) computed an analogous family of closed axisymmetric shapes parametrized by the enclosed volume, subject to a specified surface area. The direct computation of periodic stationary shapes arising from the instability of the infinite thread is the subject of ongoing research.

This research was supported National Science Foundation. Acknowledgement is made to the Donors of the Petroleum Research Fund, administered by the American Chemical Society, for partial support.

REFERENCES

Barthes-Biesel, D. 1980 Motion of a spherical microcapsule freely suspended in a linear shear flow. *J. Fluid Mech.* **100**, 831–853.

Barthes-Biesel, D. & Rallison, J. M. 1981 The time-dependent deformation of a capsule freely suspended in a linear shear flow. *J. Fluid Mech.* **113**, 251–267.

Bar-Ziv, R. & Moses, E. 1994 Instability and 'pearling' states produced in tubular membranes by competition of curvature and tension. *Phys. Rev. Lett.* **73**, 1392–1395.

Boey, S. K., Boal, D. H. & Discher, D. E. 1998*a* Simulations of the erythrocyte cytoskeleton at large deformation. I. Microscopic models. *Biophys. J.* **75**, 1573–1583.

Boey, S. K., Boal, D. H. & Discher, D. E. 1998*b* Simulations of the erythrocyte cytoskeleton at large deformation. II. Micropipette aspiration. *Biophys. J.* **75**, 1584–1597.

Breyiannis, G. & Pozrikidis, C. 1999 Simple shear flow of suspensions of elastic capsules. *Theor. Comput. Fluid Dyn.* (in press).

Eggers, J. 1997 Nonlinear dynamics and breakup of free-surface flows. *Rev. Mod. Phys.* **69**, 865–930.

Eggleton, C. D. & Popel, A. S. 1998 Large deformation of red blood cell ghosts in a simple shear flow. *Phys. Fluids* **10**, 1834–1845.

Evans, E. & Yeung, A. 1994 Hidden dynamics in rapid changes of bilayer shape. *Chem. Phys. Lipids* **73**, 39–56.

Goren, S. L. 1962 The instability of an annular thread of fluid. *J. Fluid Mech.* **12**, 309–319.

Green, A. E. & Adkins, J. E. 1960 *Large Elastic Deformations and Non-linear Continuum Mechanics.* Oxford University Press.

Halpern, D. & Grotberg, J. B. 1992 Fluid-elastic instabilities of liquid-lined flexible tubes. *J. Fluid Mech.* **244**, 615–632.

Halpern, D. & Grotberg, J. B. 1993 Surfactant effects on fluid-elastic instabilities of liquid-lined flexible tubes: A model of airway closure. *J. Biomed. Engng* **115**, 271–277.

Heil, M. 1997 Stokes flow in collapsible tubes: computation and experiment. *J. Fluid Mech.* **353**, 285–312.

Heil, M. 1998 Stokes flow in an elastic tube – A large-displacement fluid-structure interaction problem. *Intl J. Numer. Meth. Fluids* **28**, 243–265.

Heil, M. 1999*a* Minimal liquid bridges in non-axisymmetrically buckled elastic tubes. *J. Fluid Mech.* **380**, 309–337.

Heil, M. 1999*b* Airway closure: Occluding liquid bridges in strongly buckled elastic tubes. *Trans. ASME J. Biomech. Engng* **121**, 487–493.

Kraus, M. Wintz, W. Seifert, U. & Lipowsky, R. 1996 Fluid vesicles in shear flow. *Phys. Rev. Lett.* **77**, 3685–3688.

Kwak, S. & Pozrikidis, C. 1999 Effect of surfactants on the instability of a liquid thread or annular layer. Part 1. Quiescent fluids. Submitted.

Li, X. Z., Barthes-Biesel, D. & Helmy, A. 1988 Large deformation and burst of a capsule freely suspended in an elongational flow. *J. Fluid Mech.* **187**, 179–196.

Lin, S. P. & Reitz, R. D. 1998 Drop and spray formation from a liquid jet. *Ann. Rev. Fluid Mech.* **30**, 85–105.

Lipowsky, R. 1991 The conformation of membranes. *Nature* **349**, 475–481.

Longuet-Higgins, M. S. & Cokelet E. D. 1976 The deformation of steep surface waves on water I. A numerical method of computation. *Proc. R. Soc. Lond.* A **350**, 1–26.

McDonald, P. 1996 *Continuum Mechanics.* PWS Press.

Mohandas, N. & Evans, E. 1994 Mechanical properties of the red cell membrane in relation to molecular structure and genetic defects. *Ann. Rev. Biophys. Biomol. Struct.* **23**, 787–818.

Navot, Y. 1998 Elastic membranes in viscous shear flow. *Phys. Fluids* **10**, 1819–1833.

Nelson, P., Powers, T. & Seifert, U. 1995 Dynamical theory of the pearling instability in cylindrical vessels. *Phys. Rev. Lett.* **74**, 3384–3387.

Papageorgiou, D. T. 1995 On the breakup of viscous liquid threads. *Phys. Fluids* **7**, 1529–1544.

Papageorgiou, D. T. 1996 Description of jet break up. In *Advances in Multi-fluid Flows* (ed. Y. Y. Renardy, A. C. Coward, D. T. Papageorgiou & S. M. Sun). SIAM.

Pedley, T. J. & Luo, X. Y. 1998 Modelling flow and oscillation in collapsible tubes. *Theor. Comput. Fluid Dyn.* **10**, 277–294.

Plateau, J. 1873 *Statique Experimentale et Theoretique des Liquides Soumis aux Seules Forces Moleculaires.* Gauthier-Villars.

Pozrikidis, C. 1990 The axisymmetric deformation of a red blood cell in uniaxial straining Stokes flow. *J. Fluid Mech.* **216**, 231–254.

Pozrikidis, C. 1992 *Boundary Integral and Singularity Methods for Linearized Viscous Flow.* Cambridge University Press.

Pozrikidis, C. 1995 Finite deformation of liquid capsules enclosed by elastic membranes in simple shear flow. *J. Fluid Mech.* **297**, 123–152.

Pozrikidis, C. 1997 *Introduction to Theoretical and Computational Fluid Dynamics.* Oxford University Press.

Pozrikidis, C. 1999 Capillary instability and breakup of liquid threads. *J. Engng Maths* **36**, 255–275.

Ramanujan, S. & Pozrikidis, C. 1998 Deformation of liquid capsules enclosed by elastic membranes: large deformations and the effect of fluid viscosities. *J. Fluid Mech.* **361**, 117–143.

Rayleigh, Lord 1878 On the instability of jets. *Proc. Lond. Math. Soc.* **10**, 4–13.

Rayleigh, Lord 1892 On the stability of a cylinder of viscous liquid under capillary force. *Phil. Mag.* **34**, 145.

Secomb, T. W. & Hsu, R. 1993 Non-axisymmetric motion of rigid closely fitting particles in fluid-filled tubes. *J. Fluid Mech.* **257**, 403–420.

Seifert, U. 1997 Configurations of fluid membranes and vesicles. *Adv. Phys.* **46**, 13–137.

Seifert, U. 1998 Fluid membranes in hydrodynamic flow fields: Formalism and an application to fluctuating quasi-spherical vesicles in shear flow. *Eur. Phys. J.* B (in press).

Tomotika, S. 1935 On the instability of a cylindrical thread of a viscous liquid surrounded by another viscous fluid. *Proc. R. Soc. Lond.* A **150**, 322–337.

Yarin, A. L. 1993 *Free Liquid Jets and Films: Hydrodynamics and Rheology*. Longman.

Zarda, P. R., Chien, S. & Skalak, R. 1977 Elastic deformations of red blood cells. *J. Biomechanics* **19**, 211–221.

Zhou, H. & Pozrikidis, C. 1995 Deformation of capsules with incompressible interfaces in simple shear flow. *J. Fluid Mech.* **283**, 175–200.